Timing of a future glaciation in view of anthropogenic climate change

Christine Kaufhold[1,2*], Matteo Willeit[1], Guy Munhoven[3], Volker Klemann[4], Andrey Ganopolski[1]

[1]Department of Earth System Analysis, Potsdam Institute for Climate Impact Research (PIK), Member of the Leibniz Association, Potsdam, 14412, Brandenburg, Germany.
[2]Institute of Physics and Astronomy, Universität Potsdam, Potsdam, 14476, Brandenburg, Germany.
[3]Dépt. d'Astrophysique, Géophysique et Océanographie, Université de Liège, Liège, 4000, Belgium.
[4]Section Earth System Modelling, Department of Geodesy, GFZ Helmholtz Centre for Geosciences, Potsdam, 14473, Brandenburg, Germany.

*Corresponding author(s). E-mail(s): kaufhold@pik-potsdam.de;
Contributing authors: willeit@pik-potsdam.de; guy.munhoven@uliege.be; volker.klemann@gfz.de; andrey.ganopolski@pik-potsdam.de;

Abstract

Human activities are expected to delay the next glacial inception because of the long atmospheric lifetime of anthropogenic CO_2. We present the first Earth system model simulations for the next 200,000 years with dynamic ice sheets and interactive atmospheric CO_2, exploring how emissions will impact a future glacial inception. Historical emissions (500 PgC) are unlikely to delay inception, expected to occur under natural conditions around 50,000 years from now, while a doubling of current emissions (1000 PgC) would delay inception for another 50,000 years. Inception is generally expected within the next 200,000 years for emissions up to 5000 PgC. Our model results show that assumptions about the long-term balance of geological carbon sources and sinks has a strong impact on the timing of the next glacial inception, while millennial-scale AMOC variability influences the exact timing. This work highlights the long-term impact of anthropogenic CO_2 on climate.

1 Introduction

Over the past 2.7 million years, Earth's climate has been characterized by glacial cycles, i.e., quasi-periodic patterns of long, cold glacials followed by shorter, warm interglacials. These Pleistocene glacial cycles were driven by seasonal variations in insolation caused by changes in orbital configuration, and shaped by internal feedbacks between ice sheets, the climate, the solid Earth [1, 2], and the carbon cycle [3]. According to Milankovitch theory, a new glacial cycle begins (i.e., glacial inception) when there is a prolonged period of low summer insolation in high-latitude regions of the Northern Hemisphere (NH). Snow that is not completely melted during summer turns into ice, and the increasing albedo reinforces ice accumulation year after year [4–7].

Although summer insolation during the Holocene has already reached its minimum, there is no sign of an imminent glacial inception despite the 100 kyr cyclicity that has persisted during the last 800 kyr. Some argue that, under hypothetical non-anthropogenic conditions, the current interglacial would have already ended [8–11]; others suggest that we were already pre-dispositioned for an interglacial longer than 10 kyr as a result of minima in the 100-kyr and 400-kyr eccentricity cycles [12–14], similar to the prolonged interglacial observed during Marine Isotope Stage 11 [15, 16]. Various estimates have been given for the potential duration of this exceptionally long interglacial. A few studies have proposed that the current interglacial would persist until $\sim$10 kyr AP (after present) [17, 18] or $\sim$20 kyr AP [19], but more often has an estimate of $\sim$40 to 60 kyr AP has been provided using a variety of modelling tools [20–29].

Considering that anthropogenic activities over the past few centuries have increased atmospheric CO_2 concentration beyond Pleistocene levels to $\sim$420 ppm [30], the natural length of the Holocene interglacial may now only be of theoretical interest. This is because atmospheric greenhouse gas concentrations, particularly CO_2, will also affect summer temperatures in the NH, and the critical insolation required to trigger glacial inception will vary with atmospheric CO_2 concentration [28, 31]. Although glacial inceptions were triggered by decreasing summer insolation over the past $\sim$1 million years, the timing of the next glacial inception will additionally depend on the amount of anthropogenic carbon emissions. This CO_2 effect is particularly relevant for the next $\sim$100 kyr because of weak orbital forcing associated with a minimum in Earth's eccentricity [32]. Given that anthropogenic CO_2 emissions will remain in the atmosphere over the coming millennia due to their long lifetime [22, 33, 34], elevated CO_2 concentrations will likely delay the onset of the next glacial period [28, 29]. Predicting the timing of the next glacial cycle under anthropogenic conditions therefore strongly depends on our ability to model long-term carbon cycle dynamics.

Despite efforts to model climate change over the next century, the long-term trajectory of the Earth system is essential for both ethical and practical reasons. From a broad perspective, such simulations help to understand the full extent of the Anthropocene –will anthropogenic impacts become negligible in a few multi-millennia, or will they fundamentally change the Earth's natural cycles on orbital timescales and beyond? On a more practical level, long-term climate projections are necessary to assess the safety of high-level radioactive waste repositories, which must remain secure for hundreds of thousands of years.

In this study we present a set of long-term transient coupled climate–carbon cycle–ice sheet model simulations under different emission scenarios for the next $\sim$200 kyrs using the fast Earth system model CLIMBER-X (Sect. 4.1). We explore how the timing of the next glacial inception depends on the magnitude of cumulative anthropogenic CO_2 emissions. We show that assumptions about the long-term balance of geological carbon sources and sinks have profound implications on the timing of the next glaciation and highlight the potentially critical role of millennial-scale variability. These are the first transient simulations of the next glacial inception under natural and anthropogenic conditions performed using a fully coupled (climate–carbon cycle–ice sheet) Earth system model.

2 Results

2.1 Effect of imbalances in the carbon cycle

Table 1 Overview of configurations used for the main experiments in this study. The procedure for obtaining values for volcanic outgassing is described in Sect. 4.2.

Experiment name	Volcanic outgassing (PgC yr^{-1})	Interactive ice sheets
PIeq	0.0706	Off
LGCeq	0.0559	Off
LGCeq_ice	0.0559	On

To project the long-term evolution of atmospheric CO_2 and climate, it is necessary to make assumptions about the initial state of the carbon cycle. The ocean and land carbon cycle can be assumed to be reasonably close to equilibrium during the pre-industrial time as a result of relatively stable conditions persisting over most of the Holocene ($\sim$12 kyr). This time is sufficiently long even for the equilibration of slow ocean biogeochemical processes (e.g., air–sea exchange, productivity, ocean circulation, etc.) and permafrost carbon. For centennial projections, carbon exchange between the atmosphere, ocean, and land is generally sufficient to consider. On multi-millennial timescales and beyond, however, the response of marine sediments becomes important, and geological sources and sinks of carbon from sediment burial and chemical weathering on land must be accounted for. In such an 'open' carbon cycle setup, an equilibrium condition of the carbon cycle implies that, on the long-term average, volcanic CO_2 outgassing has to provide half of the atmospheric CO_2 consumed by silicate weathering [35, 36]. Due to their long intrinsic timescales, these processes cannot be considered to be in equilibrium during the pre-industrial time.

Despite this, some studies investigating the long-term response of the climate assume that the pre-industrial state was in equilibrium, which implies that a constant volcanic outgassing is assumed to balance half of the pre-industrial silicate weathering rate [29, 33, 34, 37]. However, it is well established that the silicate weathering rate depends on climate, the so-called geological "thermostat" of Earth [38, 39], meaning that it is expected to vary substantially over glacial–interglacial cycles. Since most of the last $\sim$1 million years has been colder than the pre-industrial, and CO_2 concentrations have remained nearly constant when averaged over multiple glacial cycles, it is reasonable to assume that volcanic outgassing should balance the average silicate weathering rate over one or more glacial cycles.

In a set of experiments using prescribed present-day ice sheets, we apply two different constant volcanic outgassing rates to first examine how different assumptions about the pre-industrial state of the carbon cycle influence the natural (i.e., in the absence of anthropogenic emissions) evolution of simulated future atmospheric CO_2 concentrations. These rates, determined in Sect. 4.2, correspond to (1) half the estimated pre-industrial silicate weathering rate and to (2) half the average silicate weathering rate over the last glacial cycle.

In our model, the assumption that the carbon cycle is in equilibrium with pre-industrial conditions (PIeq) corresponds to a constant volcanic outgassing of 0.0706 PgC yr^{-1}. This results in simulated CO_2 concentrations which remain relatively stable for the whole simulation period of 200 kyr (Fig. 1). In the PIeq experiment, atmospheric CO_2 concentration responds to the evolving orbital configuration of the Earth, oscillating by up to $\pm$20 ppm around the long-term average of about 280 ppm (Fig. S5). The more realistic assumption where volcanic outgassing balances the average silicate weathering rate over the last glacial cycle (LGCeq) requires a constant volcanic outgassing of 0.0559 PgC yr^{-1}, which is about 20% smaller than in PIeq. This rate is similar to those used in other studies that have successfully simulated glacial cycles [3, 40, 41] and leads to a CO_2 decreasing trend induced by the pre-industrial imbalance between geological carbon sources and sinks. This leads to a substantial drift in simulated atmospheric CO_2 from PIeq within only a few tens of kyr (Fig. 1). In the LGCeq experiment, atmospheric CO_2 concentration reaches

~220 ppm after 200 kyr, and is significantly lower than in PIeq, which is ~280 ppm at this time (Fig. 1). Although we assume that the LGCeq setup is the most realistic, it should be noted that, due to poor constraints on present-day silicate weathering rates and the sensitivity of both silicate weathering and volcanic outgassing to glacial–interglacial variability [42–44], the value used for volcanic outgassing in LGCeq has significant uncertainties. Therefore, we also present results from the PIeq setup, which represents an upper bound on future CO_2 concentrations.

2.2 Natural length of the current interglacial

We use Eq. 1, the critical insolation–CO_2 relation for glacial inception [28, 31] to predict the timing of the next glaciation using the simulated atmospheric CO_2 and the well-known future evolution of maximum insolation at 65°N (smx65 in $\mathrm{Wm^{-2}}$, [32]). This is done by determining when simulated atmospheric CO_2 falls below the "inception threshold" ($CO_{2,\mathrm{cr}}$ in ppm):

$$CO_{2,\mathrm{cr}} = 280e^{(465-\mathrm{smx65})/75} \tag{1}$$

At different insolation minima over the next 200 kyr, the associated level of $CO_{2,\mathrm{cr}}$ ranges between approximately 185 ppm (at 37 kyr AP) to approximately 325 ppm (at 170 kyr AP) (Table S1). The relation suggests that, under present-day insolation conditions, an imminent glacial inception would only be possible if CO_2 concentration drops below approximately 235 ppm (Table S1), demonstrating that the current climate is far from conditions required for glacial inception. Present-day inception thresholds for CO_2 concentration identified by other studies (e.g., 210 ppm [20], 245 ppm [45], or 270 ppm [23]) would not be crossed either. For the PIeq experiment, glacial inception under the natural evolution of the Earth system (i.e., the "natural timing" of glacial inception) is predicted to occur around 126 kyr AP, with a CO_2 concentration of approximately 285 ppm (Fig. 2d, Table A2). For the LGCeq experiment, the natural timing changes significantly, and glacial inception is predicted to occur around 52 kyr AP with a CO_2 concentration of approximately 260 ppm (Fig. 2e, Table A2). This aligns with some previous estimates placing the next glacial inception at around 50 kyr AP [20, 22–26, 28, 29].

To evaluate our prediction for the natural timing of glacial inception, done using Eq. 1, we repeat the LGCeq simulation with interactive ice sheets (LGCeq_ice) in the NH. For this, we consider a doubling of present-day NH ice sheet area as our criterion for a simulated glacial inception (Sect. 4.4). Over the first 40 kyr of the simulation, some high-altitude areas become glaciated (e.g., Baffin Mountains, Fig. 4a) due to successive insolation minima at ~17 kyr and ~37 kyr (Table S1). However, more sites become nucleated around 45 kyr AP (Fig. 3c), and global mean sea-level, which remained nearly constant for the first ~40 kyr of the simulation, starts to fall at this time due to an increase in ice volume (Fig. 3d). This sea-level fall is particularly heterogeneous, due to the 3D Earth structure employed from ref. [46] (Fig. 4a). Millennial-scale variability in the Atlantic Meridional Overturning Circulation (AMOC) also begins around 45 kyr AP (Fig. 3b, Fig. A6a, h) and closely resembles past Dansgaard–Oeschger (DO) events [47, 48] which are realistically reproduced by CLIMBER-X [49]. The abrupt weakening of the AMOC into a Stadial state leads to a reduction in the northward transport of warm surface waters and an expansion of sea ice (Fig. A5). This causes widespread cooling in the northern North Atlantic, thereby facilitating the formation of these additional nucleation sites and the lateral expansion of NH ice sheets. The effect of AMOC-induced summer cooling dominates over the decrease in annual precipitation, and leads to a net increase of the surface mass balance over ice sheets (Fig. A5).

The simulated natural timing of glacial inception generally agrees well with the predicted timing determined by the critical insolation-CO_2 relation, with a doubling of NH ice area by ~52 kyr AP (Fig. 3c, Table A2). At this time, ice area rapidly increases over the Canadian Arctic Archipelago and Scandinavian Mountains (Fig. 4d, g). Widespread ice sheet growth at nucleation sites over Svalbard, Franz Josef Land, Novaya Zemlya, Scandinavian Mountains, and the Pacific and Arctic Cordillera coalesce into the Barents, Fennoscandian, Cordilleran, Innuitian and Foxe–Baffin ice sheets. This is consistent with patterns of ice sheet development during the last glacial cycle in North America and Eurasia [50–54]. Following this, ice sheets in

North America and Eurasia merge by 53 kyr AP, demonstrating the formation of future North American and European Ice Sheet Complexes (Fig. A1). Following inception, relative sea-level rises around the ice sheets due to an increased gravitational attraction and regional subsidence by the growing ice sheets, while sea-level falls in the far field due to the accumulation of ice on land (Fig. 4g). The forebulge surrounding the subsiding regions reduce sea level, and is most pronounced in regions where the considered mantle viscosity is small, e.g., in the mid-Atlantic, and at the northwestern Pacific coast.

2.3 Anthropogenic global warming and the next glaciation

Anthropogenic activities are projected to further raise atmospheric CO_2 levels and global temperatures. In the absence of significant carbon dioxide removal efforts, it is expected that the land and ocean in combination will absorb up to ∼60% of emissions [33, 34, 55, 56], leading to a sharp decline in atmospheric CO_2 concentrations over the first millennium after anthropogenic emissions cease. On longer timescales, however, the climate–silicate weathering feedback will control the lifetime of anthropogenic CO_2 [34], shaping the Earth's long-term carbon cycle response. In the LGCeq experiment, this is combined with a CO_2 decreasing trend, as the pre-industrial state not in equilibrium and weathering is not compensated by volcanic outgassing. This results in atmospheric CO_2 concentrations returning to pre-industrial levels faster than in some previous studies [22, 37], bringing the Earth system closer to the inception threshold.

The timing of the next glacial inception, as predicted by Eq. 1, varies significantly depending on the level of cumulative emissions (ensemble ranging from 0-5000 PgC) and on the assumed carbon cycle (im)balance (PIeq vs. LGCeq). In the PIeq experiment, glacial inception is predicted to occur around or after ∼170 kyr AP for emission scenarios 500 PgC and larger (Fig. 2d, Table A2). In contrast, the predicted timing of glacial inception in the LGCeq experiment is more evenly distributed over the 200 kyr simulation duration during four periods of sufficiently low insolation (Fig. 2e, Table A2).

Similar to Sect. 2.2, we rerun the LGCeq experiment with interactive ice sheets (LGCeq_ice) to evaluate our prediction. Ice sheet volume in the 500 PgC scenario closely follows the natural evolution and glacial inception is simulated at approximately the same time as for the natural evolution at ∼50 kyr AP, as predicted (Fig. 3c, Fig. A7a, b). Cumulative CO_2 emissions of 1000 PgC are enough to evade inception at ∼50 kyr AP (Fig. 4h) and postpone it to ∼100 kyr AP (Fig. 3c, Fig. A7c, d). Emissions higher than 1000 PgC lead to an initial loss of the Greenland ice sheet due to a combination of high CO_2 and several insolation maxima (Fig. 3c, Fig. 4h, i). Although glacial inception in the 4000 and 5000 PgC scenarios is simulated at ∼179 kyr AP as predicted (Fig. 3c, Fig. A7i-l), it does not occur when predicted at ∼125 kyr AP for the 2000 and 3000 PgC emission scenarios (Fig. 3c). Two interconnected reasons could explain this. Not only is there a regional warming effect from the missing Greenland ice sheet (which is not accounted for in the critical CO_2–insolation relation since Eq. 1 was derived in the presence of the Greenland ice sheet), but the 2000 and 3000 PgC emission scenarios also lack millennial-scale AMOC variability at ∼125 kyr AP as atmospheric CO_2 concentrations are too high [49]. Despite this, the low insolation minimum at ∼170 kyr AP ensures that inception occurs at the latest during that time, at least for emissions up to 5000 PgC (Fig. 3c, Table A2). The spatial patterns of ice sheet growth during glacial inception is similar to that of the natural evolution, with an initial ice nucleation over high altitude sites, followed by widespread expansion and thickening of ice sheets (Fig. A7).

3 Discussion

We presented the first, fully coupled climate–carbon cycle–ice sheets model simulations for the next 200,000 years and investigated how the timing of the next glacial inception varies under different scenarios of cumulative anthropogenic carbon emissions. For emissions of 500 PgC and less, glacial inception is simulated around 50 kyr AP, while a doubling of present-day emissions (∼1000 PgC) would delay inception at the 50 kyr AP insolation minimum to approximately

100 kyr AP. Although historical carbon emissions have already contributed ∼500 PgC in cumulative emissions, low-emission scenarios with net negative emissions (e.g., SSP1-2.6, SSP4-3.4, SSP5-3.4-OS) are projected to result in similar levels of cumulative emissions (Fig. S4). To further frame this in the context of climate policy, cumulative emissions are expected to reach 1000 PgC by approximately ∼2070 in intermediate-emission scenarios such as SSP2-4.5 and as early as ∼2050 in high-emission scenarios like SSP5-8.5 (Fig. S4). Our study shows that the next glacial inception will likely occur before 200 kyr AP in all emission scenarios (up to 5000 PgC) when accounting for the long-term CO_2 decreasing trend resulting from the imbalance between geological carbon sinks and sources (Fig. 2e). If this trend is not accounted for, glacial inception is predicted to occur by the 170 kyr AP insolation minimum at the latest for all emission scenarios less than 5000 PgC (Fig. 2d). This is because insolation is substantially lowered at this time, allowing glacial inception to be triggered even at relatively high CO_2 concentrations of ∼325 ppm.

Both the predicted and simulated timing of glacial inception are in agreement with some previous studies [28, 57], but are notably different than others, whose results suggest that even intermediate emissions could postpone glacial inception for up to 500 kyr [29, 37]. There are two reasons for this. First, the strength of the silicate weathering feedback in CLIMBER-X, while within range of other models, is relatively strong and falls on the higher end of the spectrum [34]. Secondly, the latter studies made the implicit assumption that the carbon cycle was in equilibrium during the pre-industrial time, such that atmospheric CO_2 concentration would eventually return to and remain around 280 ppm following an anthropogenic perturbation. This assumption is equivalent to the one made in the PIeq experiment, where there is no negative trend in the long-term CO_2 evolution due to the carbon cycle imbalance arising between outgassing and weathering (Fig. 2d).

The simulated timing of the next glaciation is generally well predicted by the critical CO_2–insolation relation [28, 31], except for two scenarios where the Greenland ice sheet is initially melted and fails to regrow before glaciation starts in other parts of the NH due to its hysteresis behaviour [58–60]. This is to be expected, as the critical insolation–CO_2 relation was derived under the implicit assumption of an ice-covered Greenland. An ice-free Greenland would warm the climate in inception regions, thus requiring lower CO_2 concentrations to trigger widespread glaciation. Future AMOC variability is also shown to influence the timing of the next glacial inception, suggesting a potential causal relationship between rapid climate shifts in the North Atlantic and the onset of glaciations (Figs. A6, S2, S3). Sediment core data partly confirms this behaviour, as strong millennial-scale climate variability has almost always occurred after the end of each interglacial stage [61]. A potential role of AMOC weakening for the last glaciation has also been suggested by different modelling studies [62–64]. AMOC variability is likely to play a more significant role in facilitating a future glacial inception than it did for many past glacial inceptions. This is because insolation minima in the coming ∼150 kyrs are comparatively weak (Fig. 2c), and low CO_2 concentrations will be required to trigger glacial inception, which in turn implies a more unstable AMOC [49].

The timing of the next glacial inception strongly depends on the long-term trends in atmospheric CO_2 that can result from imbalances between geological sources and sinks of carbon which remain uncertain. For example, present-day values for silicate weathering and volcanic outgassing, and the response of weathering to climate change remains poorly constrained [42–44]. Furthermore, while silicate weathering is still considered to be the primary regulator of Earth's climate on long timescales, it is still not clear if other processes like phosphorus weathering fluxes and organic carbon burial could comparably influence the long-term carbon cycle [33, 65]. As uncertainties in climate sensitivity and in the representation of other carbon cycle processes will also affect the long-term CO_2 and climate evolution [34], so too are they expected to influence the timing of the next glaciation.

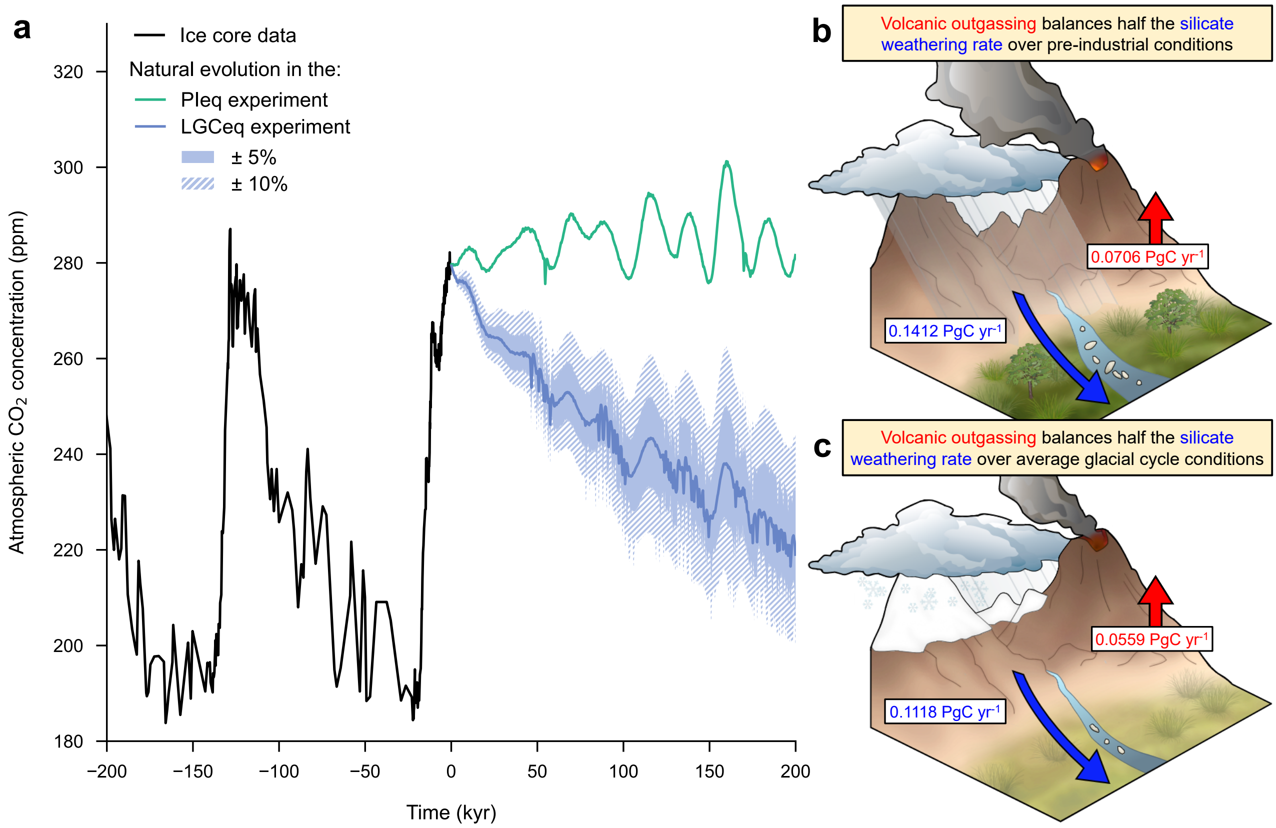

Fig. 1 The natural evolution of atmospheric CO_2 concentration. Here, we demonstrate the resulting long-term trend in atmospheric CO_2 evolution due to the carbon cycle imbalance arising between outgassing and weathering (PIeq vs. LGCeq), leading to significantly different climate evolutions over the 200 kyr period. The assumption that the carbon cycle is in equilibrium with average glacial cycle conditions (LGCeq) necessitates a constant volcanic outgassing of 0.0559 PgC yr^{-1} which produces a negative decreasing trend in atmospheric CO_2. However, given significant uncertainties in this value, we simulated future atmospheric CO_2 concentrations for values which are $\pm$5–10% the constant volcanic outgassing used in LGCeq. In light of this, we also consider the assumption that the carbon cycle is in equilibrium with pre-industrial conditions (PIeq) to be an upper bound on plausible future CO_2 concentrations, which necessitates a constant volcanic outgassing of 0.0706 PgC yr^{-1}. The proxy record (black) shows a reconstruction of atmospheric CO_2 concentration from the EPICA Dome C and Vostok ice cores [66]. A 300-year rolling mean was applied to the simulated data shown here for visibility. Sketches (b, c) were created in part using modified images from the UMCES IAN Media Library under a Creative Commons license CC BY-SA 4.0.

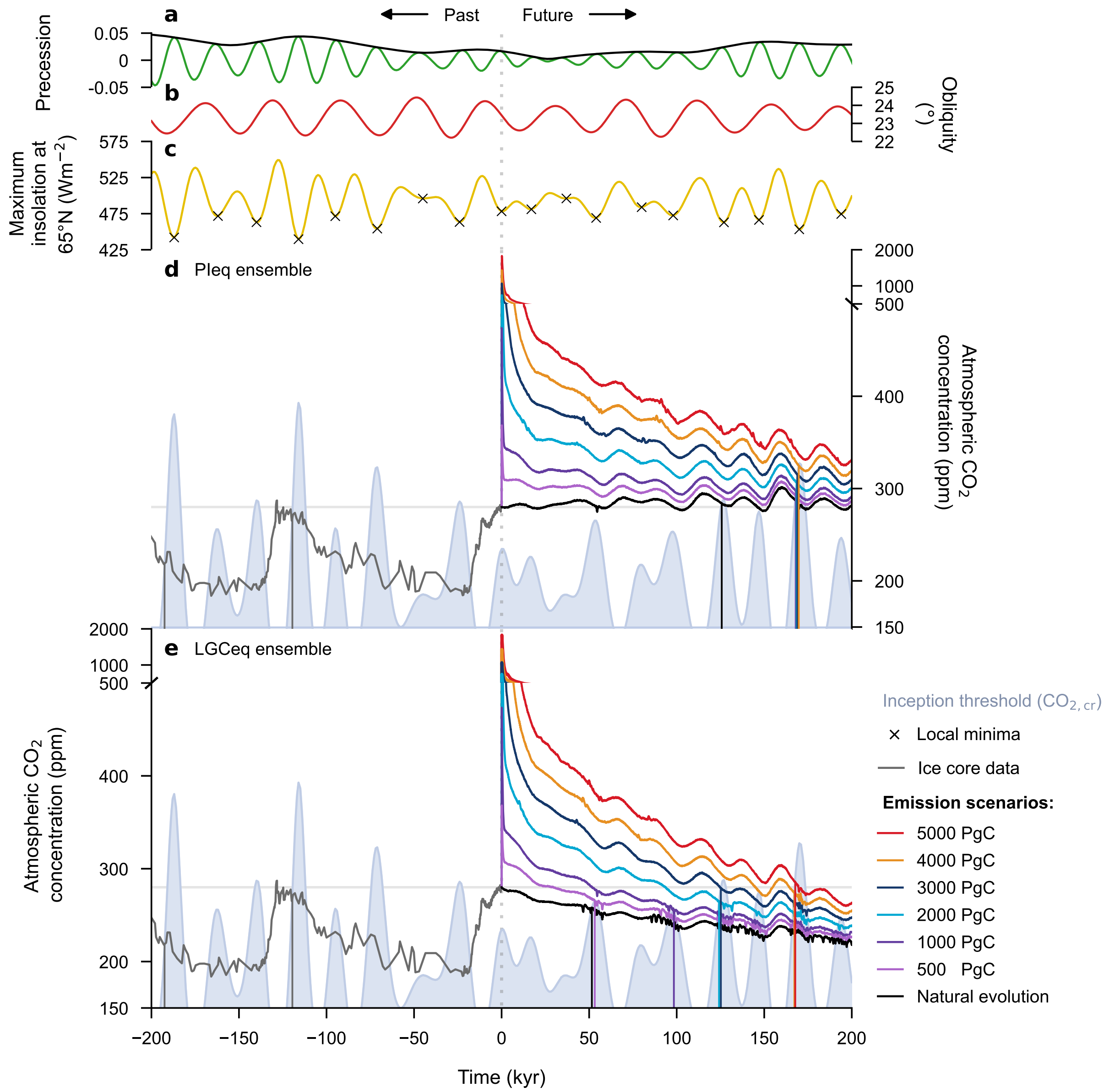

Fig. 2 Planetary and climatic conditions over the past and future 200 kyr. The orbital parameters of (a) eccentricity modulated precession and (b) obliquity have been taken from Laskar et al. (2004) [32]. The maximum annual insolation at 65°N in (c) was also taken from Laskar et al. (2004) [32]. Atmospheric CO_2 concentrations over the last 200 kyr (grey) in (d, e) was taken from the EPICA Dome C and Vostok ice cores [66]. The glacial inception threshold (light blue) was calculated using Eq. 1. Future CO_2 concentrations were plotted for the (d) PIeq ensemble and (e) the LGCeq ensemble. The vertical lines in (d, e) correspond to the predicted timing of glacial inceptions (Table A2).

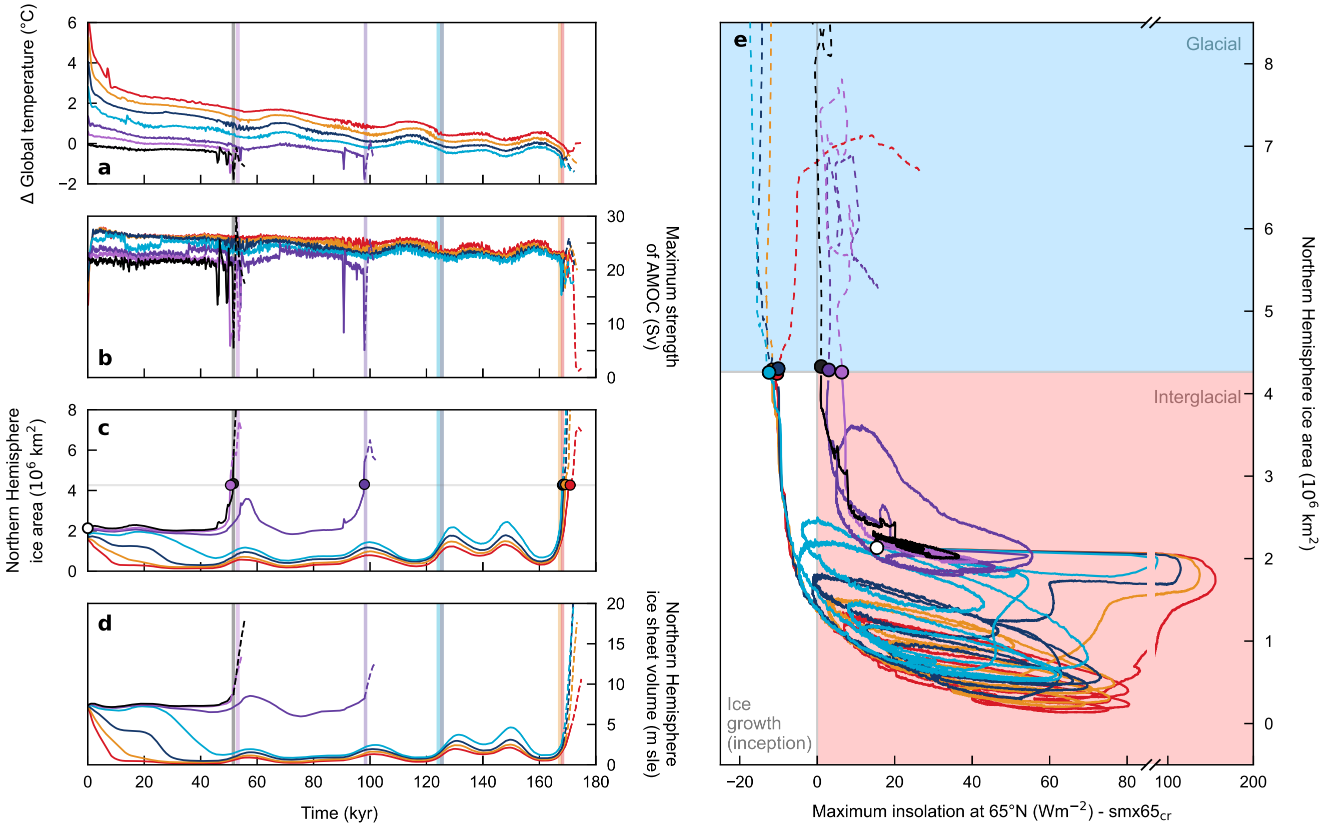

Fig. 3 The timing of the next glaciation in coupled ice-sheet experiments in an ensemble of different emission scenarios. This figure depicts NH ice sheet and climate conditions from the LGCeq_ice experiment. Colours for the timeseries and trajectories here correspond to the different emission scenarios shown in Fig. 2. The simulated (a) change in global mean temperature from the pre-industrial, (b) maximum strength of the AMOC, (c) NH ice sheet area, and (d) NH ice sheet volume in m sle (meters sea-level equivalent) is shown. In (e), the evolution of simulated ice area as a function of the difference between maximum summer insolation and smx65$_{cr}$ (the "critical insolation" for glacial inception, determined by inverting Eq. 1 and using simulated atmospheric CO_2 concentration) is presented, showing trajectories corresponding to the different emission scenarios. All trajectories in (e) from present-day (white marker). A crossing below 0 in the x-axis, synonymous with CO_2 crossing the inception threshold (here represented through smx65$_{cr}$), is shown here to lead to a rapid expansion of ice sheet area that puts trajectories in a glacial state. For visibility, a 300-year rolling mean was applied to (a-d), and a 30-year rolling mean was applied to (e). The predicted timing for glacial inception in the different emission scenarios (as determined using Eq. 1 and shown in Fig. 2e, Table A2) is given by the shaded vertical lines in (a-d). The simulated timing of glacial inception (Table A2) is denoted in (c, e) using coloured markers. Data is only shown here for 5 kyr after the simulated timing of glacial inception (indicated using dashed lines), as discussed in Sect. 4.3 and 4.4.

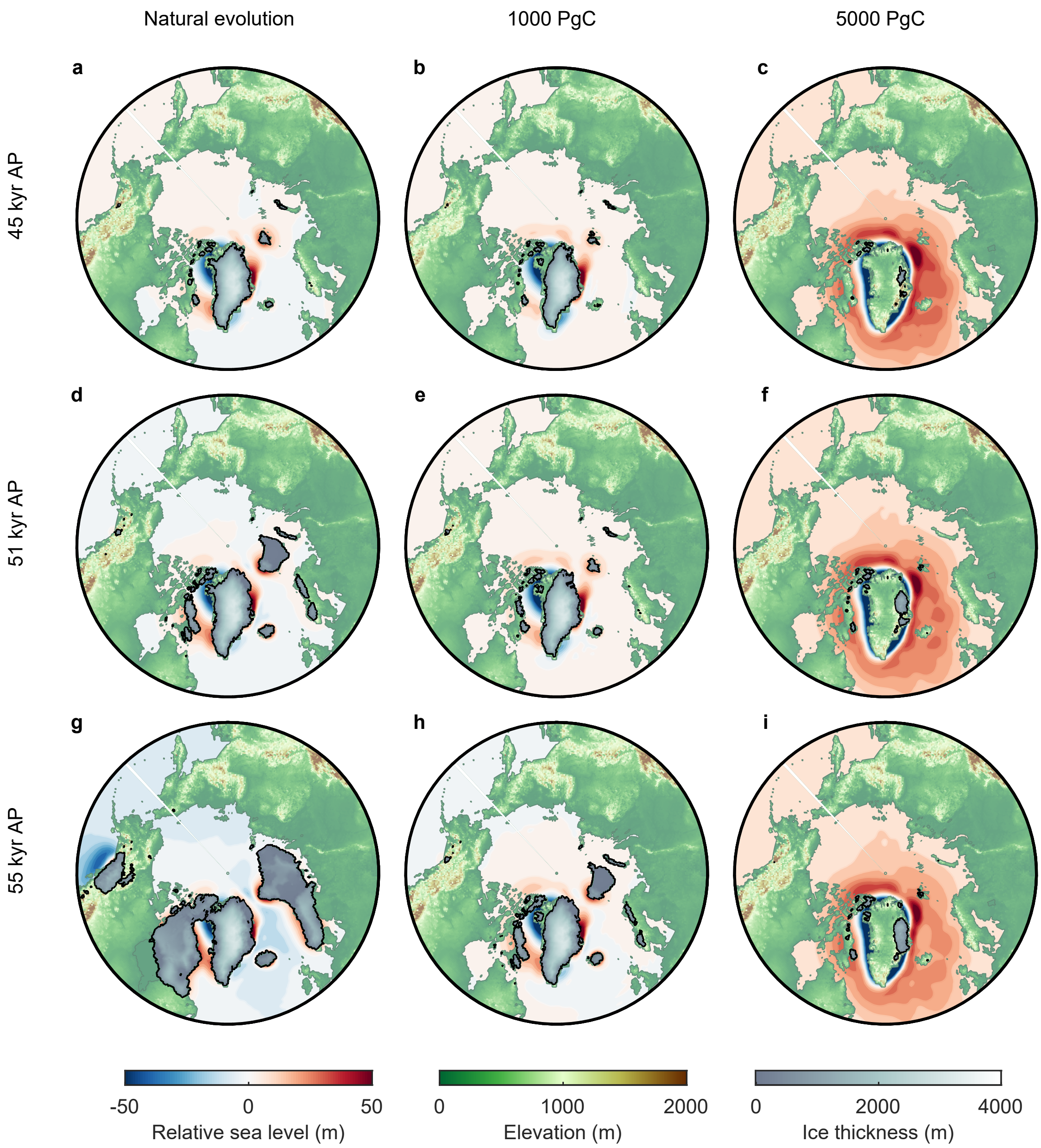

Fig. 4 Future ice sheets under different emission scenarios. The time slices of (a–c) 45 kyr AP, (d–f) 51 kyr AP, and (g–i) 55 kyr AP correspond to the timing before, during, and after the simulated natural timing of glacial inception in the LGCeq_ice experiment (∼52 kyr AP). The (a, d, g) natural evolution, (b, e, h) 1000 PgC, and (c, f, i) 5000 PgC scenarios were plotted to show the complete range of potential ice sheet evolutions, with changes in relative sea-level highlighting the effects of glacial isostatic adjustment and ice sheet melt.

4 Methods

4.1 Model

We use CLIMBER-X v1.3.0 [67], a fast Earth system model with a comprehensive representation of the global carbon cycle [36] and interactive ice sheets [68]. CLIMBER-X includes the statistical-dynamical semi-empirical atmosphere model SESAM [67], the 3D frictional-geostrophic ocean model GOLDSTEIN [69, 70], the dynamic-thermodynamic sea ice model SISIM [67], the land surface and dynamic vegetation model PALADYN [71], the biogeochemistry and marine sediments model HAMOCC [72–74], the ice sheet model SICOPOLIS [75], the surface mass balance model SEMIX [67], and the viscoelastic solid Earth model VILMA [46, 76, 77]. With the exception of SICOPOLIS, SEMIX, and VILMA, all components share a common horizontal grid at $5° \times 5°$ resolution. CLIMBER-X is a fast model and allows to simulate many realizations on long timescales. Currently, it is capable of running up to 10,000 simulation years within a single day, making it highly suitable for deep-past and deep-future Earth system modelling. The detailed carbon cycle representation allows the model to interactively simulate the atmospheric CO_2 concentration, and has already been applied to study the climate evolution over the next millennium [78], and to assess the sensitivity of the long-term carbon cycle under different cumulative emissions [34].

In experiments where we seek to describe NH ice sheets and glacial inception, we enable SICOPOLIS v5.1, VILMA, and SEMIX. SICOPOLIS uses a shallow-ice/shallow-shelf approximation for grounded and floating ice and is used to simulate NH ice sheets with a horizontal resolution of 32 km. The surface mass balance of the ice sheets is computed using the physically-based surface energy and mass balance interface SEMIX, as described in detail in Willeit et al. (2024) [68]. The viscoelastic solid Earth model VILMA accounts for changes via GIA, controlling surface displacement and sea-level. All experiments are run using the 3D mantle viscosity structure described in Bagge et al. (2021) [46]. With interactive ice sheets, CLIMBER-X has been applied to study the future evolution of the Greenland Ice Sheet [60, 79] and glacial inceptions [31], demonstrating that the model effectively replicates the last glacial inception, whilst simulating no inception during the Holocene [68].

4.2 Initialization of the carbon cycle

Since the carbon fluxes due to weathering are interactively computed in CLIMBER-X, a proper value of volcanic outgassing can be chosen to guarantee an equilibrium state of the carbon cycle with atmospheric CO_2 under any boundary conditions. In one experimental configuration, we assume that the pre-industrial (PI) carbon cycle is in equilibrium, and therefore volcanic outgassing was set to half the global silicate weathering rate at pre-industrial. This value, taken from the 100,000 year spin-up procedure as described in Willeit et al. (2023) [36], corresponds to $0.0706\,\mathrm{PgC\,yr^{-1}}$ (Fig. A4), and ensures that the atmospheric CO_2 is in equilibrium under pre-industrial conditions [35, 36]. The estimated pre-industrial silicate weathering rate ($0.1413\,\mathrm{PgC\,yr^{-1}}$) falls within observational estimates [80–83], but is notably higher than those found in previous studies on the long-term evolution of CO_2 [33, 84]. While this choice of model initialization is important to 'close' the carbon cycle and is commonly adopted in studies examining the long-term climate-carbon cycle response to anthropogenic emissions, it may not be appropriate for modelling of carbon cycle (or glacial cycles) on orbital time scales.

Since no significant long-term climate drift was observed during the past ∼1 million years, we postulate that volcanic outgassing must offset the average silicate weathering rate during the last glacial cycle (LGC). This was determined by using the simulated silicate weathering rates at the pre-industrial, described above, and determining the silicate weathering rate at the last glacial maximum (LGM) (Fig. A4). By running an equilibrium experiment under LGM conditions for 10 kyr, we determined that a rate of $0.0402\,\mathrm{PgC\,yr^{-1}}$ (corresponding to half the global silicate weathering rate calculated by CLIMBER-X at LGM, Fig. A4), would maintain atmospheric CO_2 in equilibrium at that time. This value is subject to considerable uncertainty, however, as global weathering rates during the LGM are poorly constrained, and empirical data does not offer a definitive answer as to whether or not weathering was weaker during glacial times [42, 44]. Some evidence suggests that the physical weathering from glaciers and the exposure of continental shelves may have increased weathering [82, 85–87], but these effects on the global silicate weathering rate are still poorly quantified. Therefore, we proceed with the current understanding that silicate weathering functions as a global thermostat, and that colder and drier conditions (as reported during the LGM) are expected to reduce the global weathering rates [42, 88].

We then computed an average silicate weathering rate over the LGC from the simulated PI and LGM weathering rates using the Spratt & Lisiecki (2016) sea-level stack as scaling factor [89] (Fig. A3). In a way, this scaling factor also implicitly accounts for weathering differences from the exposure of continental shelves. This approach allowed us to derive a value which represents the average volcanic outgassing over the LGC (0.0559 PgC yr^{-1}). This value is reasonably close to the corresponding values used by Brovkin et al. (2012) to simulate the last glacial cycle (0.0660 PgC yr^{-1}) [40], and Ganopolski & Brovkin (2017) to simulate the last four glacial cycles without a long-term drift (0.0636 PgC yr^{-1}) [3]. Furthermore, a $\pm$10% change in prescribed volcanic outgassing has been previously shown to cause nearly a 30 ppm drift in atmospheric CO_2 concentration over 100 kyr [3] —a pattern also seen in these experiments (Fig. 1).

4.3 Experiments

Simulations begin from a pre-industrial equilibrium state achieved through a 100,000 year spin-up of the carbon cycle model, detailed by Willeit et al. (2023) [36]. The experimental set-up here is largely inherited from Kaufhold et al. (2024) [34], but now includes evolving orbital parameters (and ice sheets, in select experiments). To investigate the effect of anthropogenic CO_2 emissions on the long-term evolution of the climate, we introduce a set of idealized CO_2 emission scenarios to create an ensemble with cumulative CO_2 emissions ranging from 500 PgC to 5000 PgC. This done through a Gaussian function over the course of $\sim$200 years (Fig. A2). The upper limit of 5000 PgC has been used in many studies as it broadly represents our maximum estimated fossil fuel reserves [90, 91]. In addition to this, we provide a run with no anthropogenic emissions (0 PgC), which we refer to as the 'natural evolution', i.e., climate evolution without anthropogenic influence.

Experiments were conducted using both the PIeq and LGCeq initializations (with the climate and carbon cycle components enabled) for different emission scenarios. Experiments with the climate, carbon cycle, and ice sheets were exclusively conducted using the LGC configuration (LGCeq_ice). As CLIMBER-X does not resolve synoptic-scale and inter-annual variability in the atmosphere and ocean, we apply Gaussian white noise in the surface ocean freshwater flux (0.50 kg m^{-2} day^{-1} amplitude) in the Atlantic (latitudinal belt between 50–80 °N) to represent the impact of such variability on the AMOC, as it was shown that this is important to properly represent millennial-scale AMOC variability in the model [49, 92]. Recognizing the critical role of temperature biases in glacial inception modelling, we introduced a 2m temperature bias correction over northern North America in the surface mass balance calculation following the method described in Ganopolski et al. (2010) [93]. The spatial distribution of this bias correction is detailed in Willeit et al. (2024) [68, in Fig. B1]. As we use the critical insolation–CO_2 relation determined in Talento et al. (2024) [31], we similarly apply a globally uniform temperature offset of $-0.5\,^{\circ}$C in the surface mass balance scheme. We make the simplification that Antarctica is prescribed by its present-day state in all simulations, assuming that its dynamics will have a negligible impact on summer temperatures over NH land (and therefore, glacial inception).

All experiments in this study run for 200,000 years, although we do not display the evolution of the LGCeq_ice experiment (e.g., in Fig 3) more than 5 kyr beyond inception as we are not yet fully confident that the complex carbon cycle response to large-scale glaciation is sufficiently well represented in CLIMBER-X. This will be evaluated in future studies investigating the CO_2 response to changes in ice sheets over the last glacial cycle. Some additional experiments were performed to assess the model drift in our experiment, the effect of different noise amplitudes in the surface ocean freshwater flux, and the effect of different noise realizations in the surface ocean freshwater flux (by recalling "random_seed" in FORTRAN). These experiments are shown in the Supplementary material. To evaluate the sensitivity of the prescribed LGCeq volcanic outgassing and its impact on atmospheric CO_2 concentrations on long timescales, we ran a set of experiments that were $\pm 5\%$ and $\pm 10\%$ the LGCeq value only for the natural evolution. A summary of all experiments is listed in Table A1.

4.4 Definition of glacial inception

Studies generally agree that glacial inception is marked by the rapid growth of ice sheets in North America [52, 54, 94, 95] and is considered a bifurcation in the climate system [6]. This latter point is significant, as it implies that there is a potential "irreversibility" of glacial inception [7]. However, this is not easily quantifiable, and only a few studies have attempted to precisely define the onset of glacial inception. Talento et al. (2024) define it as the point at which ice volume exceeds 15 m sle, roughly equivalent to twice the current ice volume of the Greenland ice sheet [31]. Similarly, Bahadory et al. (2021) use ice volume to define glacial inception, but with a threshold of 24 m sle [53]. Here, we define glacial inception as (1) the rapid expansion of ice sheets, and (2) a doubling of present-day NH ice area ($\sim 4.26 \times 10^6$ km^2). Although we do not simulate the evolution of these ice sheets through a full glacial cycle here, the simulated ice sheets should generally persist through periods of higher insolation, showing the irreversibility from an interglacial to a glacial state. In Fig. 3, ice area and volume is shown in dashed lines for a brief period following inception to highlight this persistence.

Supplementary information. Code and data used in this study is archived on Zenodo (https://doi.org/10.5281/zenodo.14861208). The CLIMBER-X model is available at https://github.com/cxesmc/climber-x/releases/tag/v1.3.0. For this study we used the tagged v1.3.0 of the model (last accessed: 27 September 2024).

Acknowledgements. CK is funded by the Bundesgesellschaft für Endlagerung through the URS project (research project no. STAFuE-21-4-Klei). MW is supported by the German paleoclimate modelling initiative PalMod (grant nos. 01LP1920B, 01LP1917D, 01LP2305B). GM is a Research Associate with the Belgian Fonds de la Recherche Scientifique–FNRS. VK is supported by the German paleoclimate modelling initiative PalMod (grant no: 01LP2305A). PalMod is part of the Research for Sustainable Development initiative (FONA) funded by the German Federal Ministry of Education and Research (BMBF). The authors gratefully acknowledge the European Regional Development Fund (ERDF), the German Federal Ministry of Education and Research, and the Land Brandenburg for supporting this project by providing resources on the high-performance computer system at the Potsdam Institute for Climate Impact Research.

Appendix A Extended material

Table A1 Overview of configurations used in all experiments performed in this study. The procedure for obtaining values for volcanic outgassing is described in Sect. 4.2.

Experiment name	Emission scenarios	Volcanic outgassing ($PgC\ yr^{-1}$)	Orbital parameters	Interactive ice sheets	Noise realization	Noise amplitude ($kg\ m^{-2}\ day^{-1}$)
			Main experiments			
PIeq	All	0.0706	On	Off	Seed 0	0.50
LGCeq	All	0.0559	On	Off	Seed 0	0.50
LGCeq_ice	All	0.0559	On	On	Seed 0	0.50
			Secondary and sensitivity experiments			
PIeq_fixed	Natural evolution	0.0706	Off	Off	Seed 0	0.00
LGCeq_p05	Natural evolution	0.0586	On	Off	Seed 0	0.50
LGCeq_m05	Natural evolution	0.0531	On	Off	Seed 0	0.50
LGCeq_p10	Natural evolution	0.0614	On	Off	Seed 0	0.50
LGCeq_m10	Natural evolution	0.0503	On	Off	Seed 0	0.50
LGCeq_seed1	Natural evolution	0.0559	On	On	Seed 1	0.50
LGCeq_seed2	Natural evolution	0.0559	On	On	Seed 2	0.50
LGCeq_seed3	Natural evolution	0.0559	On	On	Seed 3	0.50
LGCeq_seed4	Natural evolution	0.0559	On	On	Seed 4	0.50
LGCeq_seed5	Natural evolution	0.0559	On	On	Seed 5	0.50
LGCeq_n100	Natural evolution	0.0559	On	On	Seed 0	1.00
LGCeq_n025	Natural evolution	0.0559	On	On	Seed 0	0.25
LGCeq_n000	Natural evolution	0.0559	On	On	Seed 0	0.00

Table A2 The predicted and simulated timing of glacial inception for the different emission scenarios. The predicted timing (for PIeq and LGCeq) was determined using Eq. 1 and finding when simulated atmospheric CO_2 concentration crosses the inception threshold, $CO_{2,cr}$. The simulated timing (for LGCeq_ice) was determined when NH ice area increased to twice its present-day size ($\sim 4.26 \times 10^6$ km^2).

Emission scenario	Threshold-crossing time (kyr AP)	Threshold-crossing CO_2 concentration (ppm)
	PIeq	
Natural evolution	125.7	283.8
500 PgC	168.0	292.4
1000 PgC	168.0	297.5
2000 PgC	168.5	306.4
3000 PgC	168.9	315.1
4000 PgC	169.7	324.5
5000 PgC	N/A	N/A
	LGCeq	
Natural evolution	51.6	257.6
500 PgC	53.2	265.1
1000 PgC	98.4	252.2
2000 PgC	124.2	264.8
3000 PgC	125.2	279.2
4000 PgC	167.2	274.2
5000 PgC	167.7	285.4
Emission scenario	Area-doubling time (kyr AP)	Area-doubling CO_2 concentration (ppm)
	LGCeq_ice	
Natural evolution	51.6	257.2
500 PgC	50.6	267.1
1000 PgC	98.0	257.4
2000 PgC	168.2	249.9
3000 PgC	168.5	263.1
4000 PgC	169.3	269.7
5000 PgC	170.9	279.0

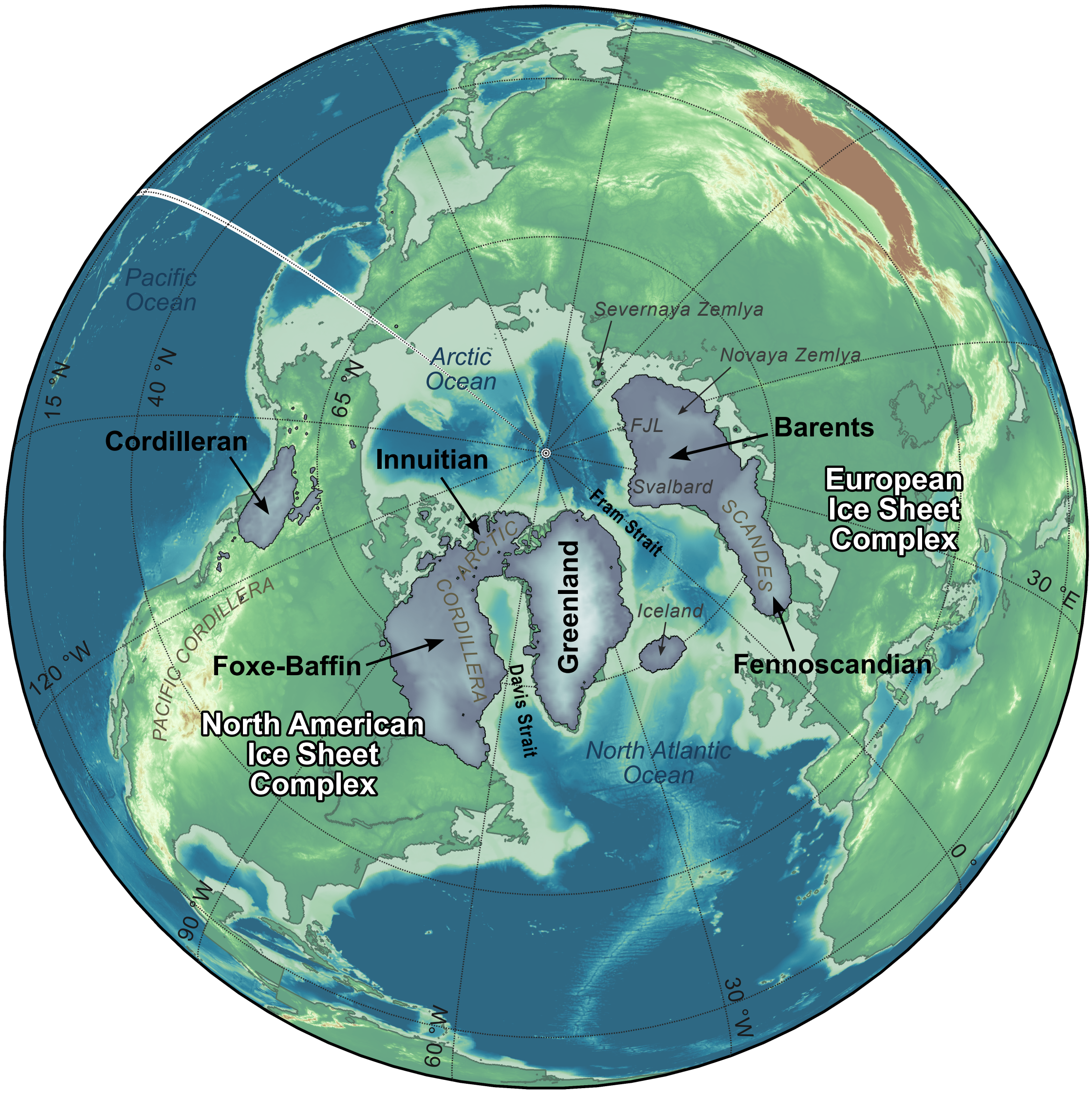

Fig. A1 **NH ice sheets under the natural evolution in the LGCeq_ice experiment at 55 kyr AP.**

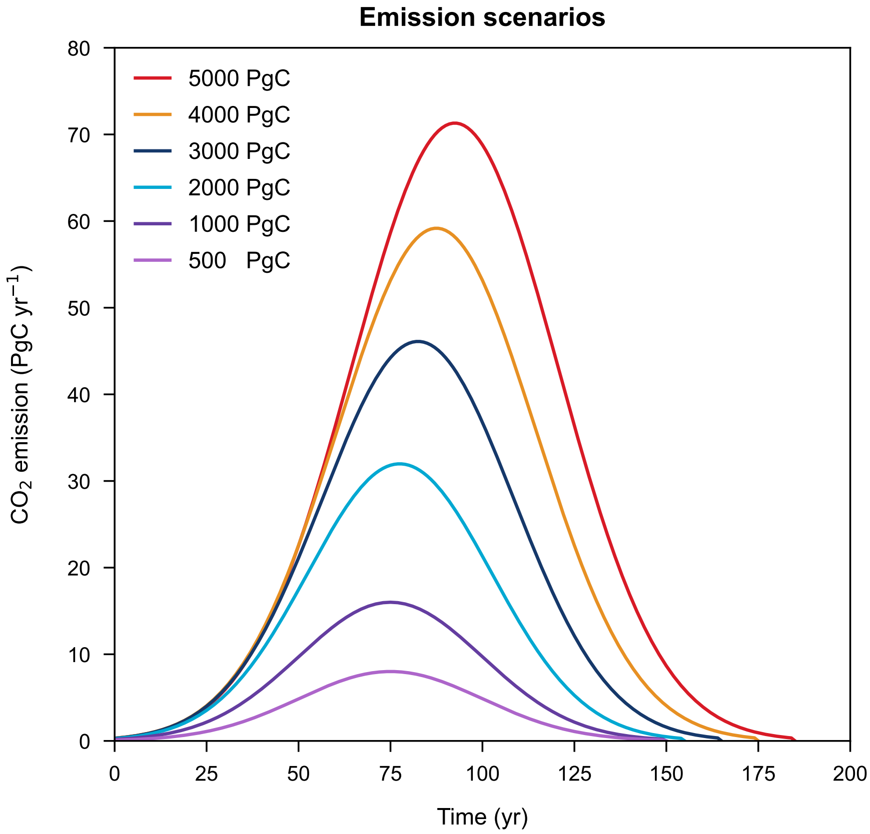

Fig. A2 Time series of prescribed CO_2 emissions. The different emission pathways were generated using a Gaussian function with an increasing mean and standard deviation, and are used to provide an ensemble of different emission scenarios. Emissions are prescribed over the first 150–180 years of the simulation, with higher cumulative emissions emitted over longer periods of time. This approach was chosen over an instantaneous pulse, commonly used in studies of the long-term forced response of the climate and carbon cycle, to maintain realism with expected emissions pathways.

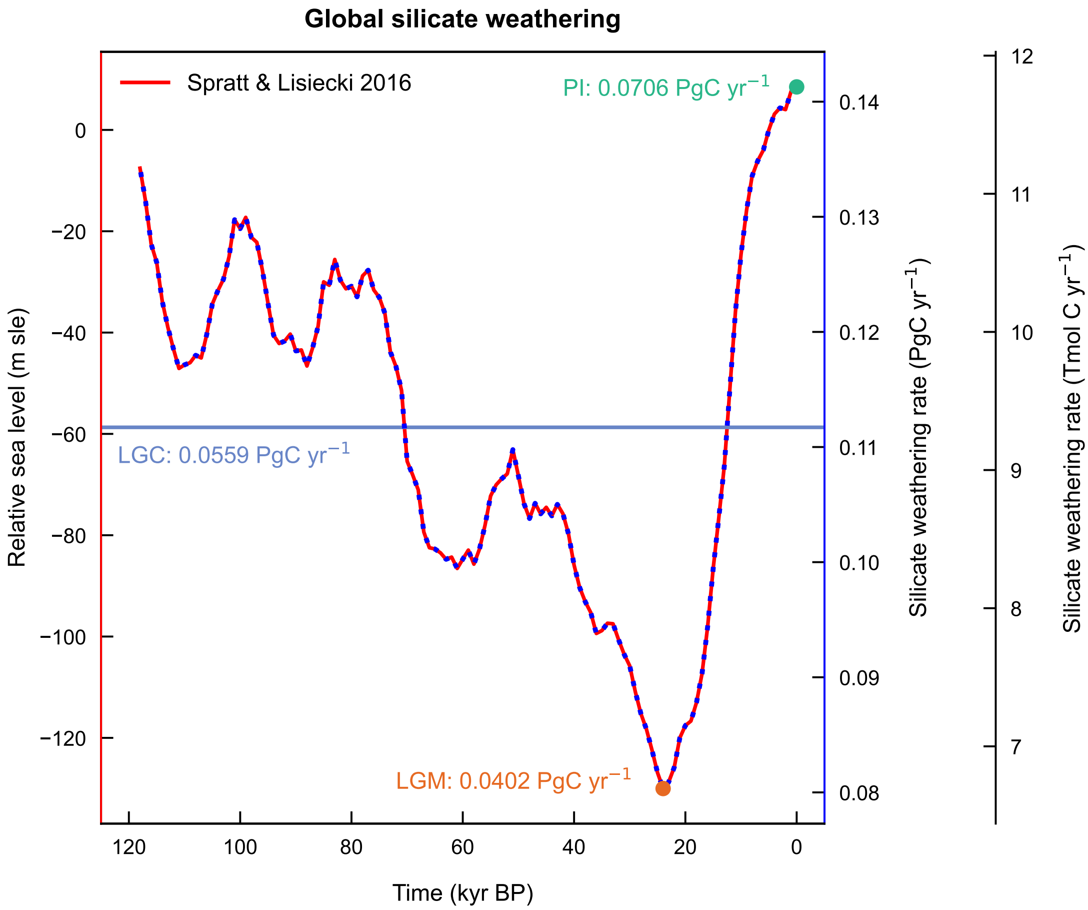

Fig. A3 Global silicate weathering rate over the last glacial cycle inferred by changes in relative sea-level. Silicate weathering rates at PI and LGM were computed via equilibrium experiments in CLIMBER-X (Fig. A4). These points were interpolated using the Spratt & Lisiecki (2016) sea-level stack [89] to provide a timeseries of global silicate weathering rates over the last glacial cycle. This timeseries was then averaged to find an average silicate weathering rate over the last glacial cycle. The determined value corresponds approximately to the average between the PI and LGM global silicate weathering rates.

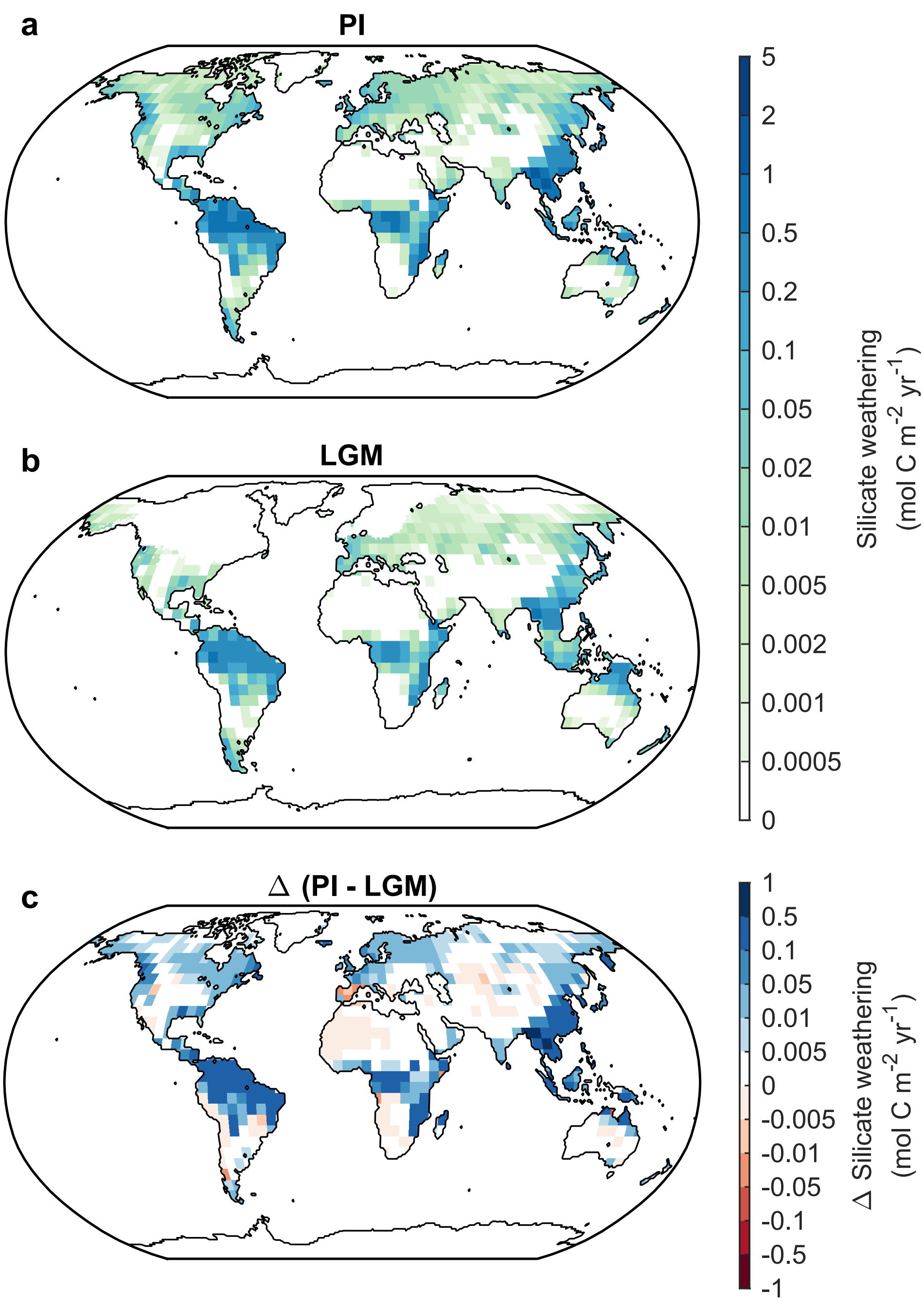

Fig. A4 Distribution of silicate weathering rates for (a) the pre-industrial, (b) the last glacial maximum, and (c) the difference between the two. The maps of the rates have been used to estimate global silicate weathering rates in Fig. A3.

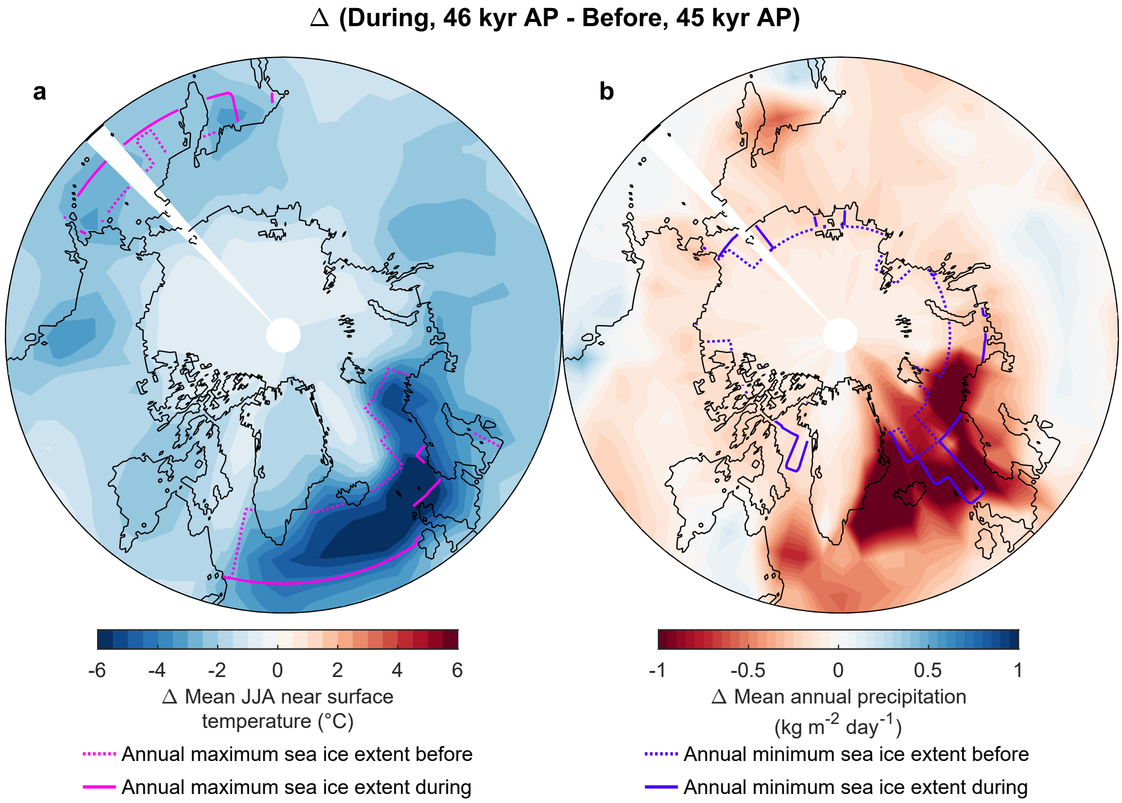

Fig. A5 Changes in (a) mean JJA near surface temperature, and (b) mean annual precipitation after the first AMOC weakening in the natural scenario. Data was taken from the LGC_ice experiment (and corresponds to the time shown in Fig. 3a-d). The annual maximum sea ice extent (in magenta), and annual minimum sea ice extent (in indigo) is shown for both the time before and during the first AMOC weakening.

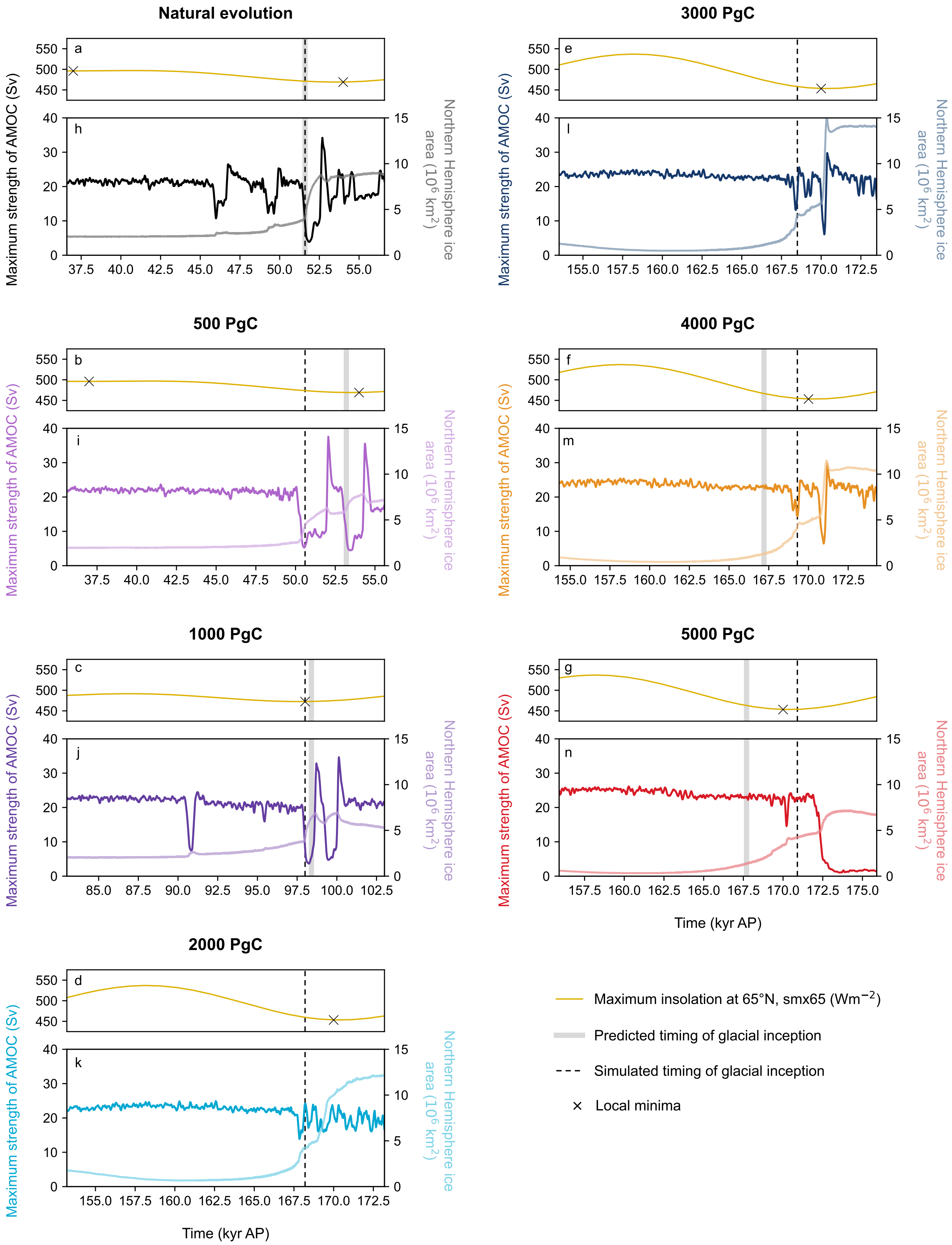

Fig. A6 Behaviour of NH ice sheet area and AMOC during the simulated glacial inception. Data was taken from the LGCeq_ice experiment. The 15 kyr leading up to the simulated glacial inception (black dashed lines, Table A2), and the 5 kyr following it, are plotted. Data is cut ∼5 kyr after inception, as discussed in Sect. 4.3 and 4.4. Maximum summer insolation [32] is shown in (a-g) to highlight the influence of insolation minima. The predicted timing of glacial inception is also provided for comparison (grey vertical lines, Table A2).

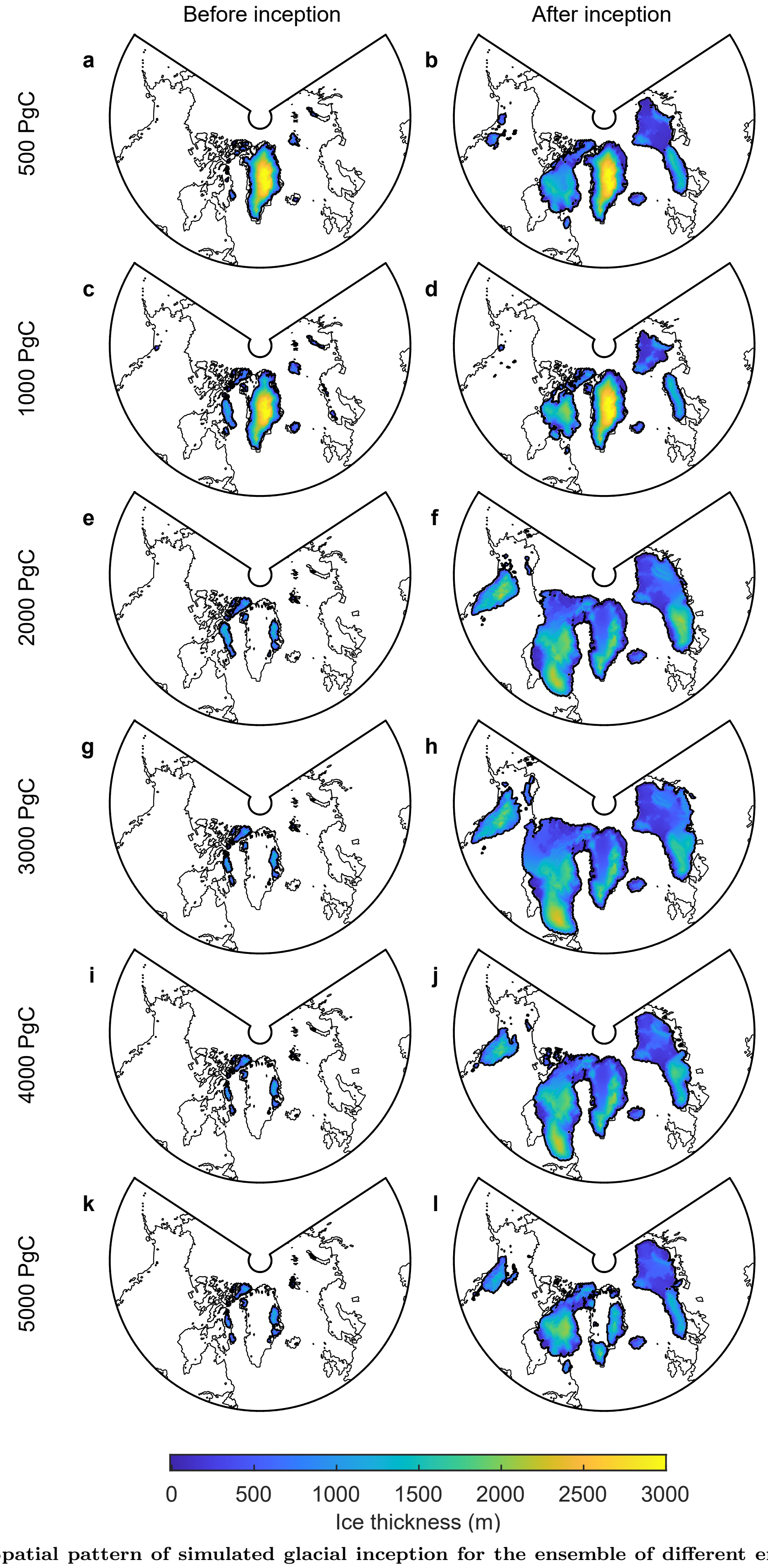

Fig. A7 Spatial pattern of simulated glacial inception for the ensemble of different emission scenarios. Data was taken from the LGCeq_ice experiment. Inception corresponds to the timing listed in Table A2, rounded to the nearest 1 kyr. The period before inception is shown for 5 kyr prior to this timestamp, while the period after inception shows 5 kyr after it.

References

[1] Ganopolski, A., Calov, R.: The role of orbital forcing, carbon dioxide and regolith in 100 kyr glacial cycles. Climate of the Past **7**(4), 1415–1425 (2011) https://doi.org/10.5194/cp-7-1415-2011

[2] Abe-Ouchi, A., Saito, F., Kawamura, K., Raymo, M.E., Okuno, J., Takahashi, K., Blatter, H.: Insolation-driven 100,000-year glacial cycles and hysteresis of ice-sheet volume. Nature **500**(7461), 190–193 (2013) https://doi.org/10.1038/nature12374

[3] Ganopolski, A., Brovkin, V.: Simulation of climate, ice sheets and CO_2 evolution during the last four glacial cycles with an Earth system model of intermediate complexity. Climate of the Past **13**(12), 1695–1716 (2017) https://doi.org/10.5194/cp-13-1695-2017

[4] Milankovitch, M.: Kanon der Erdbestrahlung und Seine Anwendung Auf Das Eiszeitenproblem vol. 33, p. 633. Spec. Publ. 132, R. Serbian Acad., Belgrade (1941)

[5] Raymo, M.E., Huybers, P.: Unlocking the mysteries of the Ice Ages. Nature **451**, 284–285 (2008) https://doi.org/10.1038/nature06589

[6] Calov, R., Ganopolski, A., Claussen, M., Petoukhov, V., Greve, R.: Transient simulation of the last glacial inception. Part I: Glacial inception as a bifurcation in the climate system. Climate Dynamics **24**(6), 545–561 (2005) https://doi.org/10.1007/s00382-005-0007-6

[7] Ganopolski, A.: Toward generalized Milankovitch theory (GMT). Climate of the Past **20**(1), 151–185 (2024) https://doi.org/10.5194/cp-20-151-2024

[8] Ruddiman, W.F.: The Anthropogenic greenhouse era began thousands of years ago. Climatic Change **61**(3), 261–293 (2003) https://doi.org/10.1023/B:CLIM.0000004577.17928.fa

[9] Broecker, W.S.: The end of the present interglacial: How and when? Quaternary Science Reviews **17**(8), 689–694 (1998) https://doi.org/10.1016/S0277-3791(98)00037-7

[10] Müller, U.C., Pross, J.: Lesson from the past: Present insolation minimum holds potential for glacial inception. Quaternary Science Reviews **26**(25), 3025–3029 (2007) https://doi.org/10.1016/j.quascirev.2007.10.006

[11] Tzedakis, P.C., Channell, J.E.T., Hodell, D.A., Kleiven, H.F., Skinner, L.C.: Determining the natural length of the current interglacial. Nature Geoscience **5**(2), 138–141 (2012) https://doi.org/10.1038/ngeo1358

[12] Paillard, D.: The timing of Pleistocene glaciations from a simple multiple-state climate model. Nature **391**(6665), 378–381 (1998) https://doi.org/10.1038/34891

[13] Berger, A., Loutre, M.F.: An exceptionally long interglacial ahead? Science **297**(5585), 1287–1288 (2002) https://doi.org/10.1126/science.1076120

[14] Berger, A., Loutre, M.F., Crucifix, M.: The Earth's climate in the next hundred thousand years (100 kyr). Surveys in Geophysics **24**, 117–138 (2003) https://doi.org/10.1023/A:1023233702670

[15] Loutre, M.F., Berger, A.: Marine Isotope Stage 11 as an analogue for the present interglacial. Global and Planetary Change **36**(3), 209–217 (2003) https://doi.org/10.1016/S0921-8181(02)00186-8

[16] Yin, Q.Z., Berger, A.: Interglacial analogues of the Holocene and its natural near future. Quaternary Science Reviews **120**, 28–46 (2015) https://doi.org/10.1016/j.quascirev.2015.04.008

[17] Vettoretti, G., Peltier, W.R.: The impact of insolation, greenhouse gas forcing and ocean circulation changes on glacial inception. The Holocene **21**(5), 803–817 (2011) https://doi.org/10.1177/0959683610394885

[18] Barker, S., Lisiecki, L.E., Knorr, G., Nuber, S., Tzedakis, P.C.: Distinct roles for precession, obliquity, and eccentricity in Pleistocene 100-kyr glacial cycles. Science **387**(6737), 3491 (2025) https://doi.org/10.1126/science.adp3491

[19] Mörner, N.-A.: When will the present interglacial end? Quaternary Research **2**(3), 341–349 (1972) https://doi.org/10.1016/0033-5894(72)90056-7

[20] Loutre, M.F., Berger, A.: Future climatic changes: Are we entering an exceptionally long interglacial? Climatic Change **46**(1), 61–90 (2000) https://doi.org/10.1023/A:1005559827189

[21] Paillard, D.: Glacial cycles: Toward a new paradigm. Reviews of Geophysics **39**(3), 325–346 (2001) https://doi.org/10.1029/2000RG000091

[22] Archer, D., Ganopolski, A.: A movable trigger: Fossil fuel CO_2 and the onset of the next glaciation. Geochemistry, Geophysics, Geosystems **6**(5), 1–7 (2005) https://doi.org/10.1029/2004GC000891

[23] Cochelin, A.-S.B., Mysak, L.A., Wang, Z.: Simulation of long-term future climate changes with the green McGill paleoclimate model: The next glacial inception. Climatic Change **79**(3), 381–401 (2006) https://doi.org/10.1007/s10584-006-9099-1

[24] Mysak, L.A.: Glacial inceptions: Past and future. Atmosphere-Ocean **46**(3), 317–341 (2008) https://doi.org/10.3137/ao.460303

[25] Crucifix, M., Rougier, J.: On the use of simple dynamical systems for climate predictions. The European Physical Journal Special Topics **174**(1), 11–31 (2009) https://doi.org/10.1140/epjst/e2009-01087-5

[26] Herrero, C., García-Olivares, A., Pelegrí, J.L.: Impact of anthropogenic CO_2 on the next glacial cycle. Climatic Change **122**(1–2), 283–298 (2013) https://doi.org/10.1007/s10584-013-1012-0

[27] Haqq-Misra, J.: Damping of glacial-interglacial cycles from anthropogenic forcing. Journal of Advances in Modeling Earth Systems **6**(3), 950–955 (2014) https://doi.org/10.1002/2014MS000326

[28] Ganopolski, A., Winkelmann, R., Schellnhuber, H.J.: Critical insolation–CO_2 relation for diagnosing past and future glacial inception. Nature **534**(7607), 19–20 (2016) https://doi.org/10.1038/nature18452

[29] Talento, S., Ganopolski, A.: Reduced-complexity model for the impact of anthropogenic CO_2 emissions on future glacial cycles. Earth System Dynamics **12**(4), 1275–1293 (2021) https://doi.org/10.5194/esd-12-1275-2021

[30] Friedlingstein, P., O'Sullivan, M., Jones, M.W., Andrew, R.M., Bakker, D.C.E., Hauck, J., Landschützer, P., Le Quéré, C., Luijkx, I.T., Peters, G.P., Peters, W., Pongratz, J., Schwingshackl, C., Sitch, S., Canadell, J.G., Ciais, P., Jackson, R.B., Alin, S.R., Anthoni, P., Barbero, L., Bates, N.R., Becker, M., Bellouin, N., Decharme, B., Bopp, L., Brasika, I.B.M., Cadule, P., Chamberlain, M.A., Chandra, N., Chau, T.-T.-T., Chevallier, F., Chini, L.P., Cronin, M., Dou, X., Enyo, K., Evans, W., Falk, S., Feely, R.A., Feng, L., Ford, D.J., Gasser, T., Ghattas, J., Gkritzalis, T., Grassi, G., Gregor, L., Gruber, N., Gürses, O., Harris, I., Hefner, M., Heinke, J., Houghton, R.A., Hurtt, G.C., Iida, Y., Ilyina, T., Jacobson, A.R., Jain, A., Jarníková, T., Jersild, A., Jiang, F., Jin, Z., Joos, F., Kato, E., Keeling, R.F., Kennedy, D.,

Klein Goldewijk, K., Knauer, J., Korsbakken, J.I., Körtzinger, A., Lan, X., Lefèvre, N., Li, H., Liu, J., Liu, Z., Ma, L., Marland, G., Mayot, N., McGuire, P.C., McKinley, G.A., Meyer, G., Morgan, E.J., Munro, D.R., Nakaoka, S.-I., Niwa, Y., O'Brien, K.M., Olsen, A., Omar, A.M., Ono, T., Paulsen, M., Pierrot, D., Pocock, K., Poulter, B., Powis, C.M., Rehder, G., Resplandy, L., Robertson, E., Rödenbeck, C., Rosan, T.M., Schwinger, J., Séférian, R., Smallman, T.L., Smith, S.M., Sospedra-Alfonso, R., Sun, Q., Sutton, A.J., Sweeney, C., Takao, S., Tans, P.P., Tian, H., Tilbrook, B., Tsujino, H., Tubiello, F., Werf, G.R., Ooijen, E., Wanninkhof, R., Watanabe, M., Wimart-Rousseau, C., Yang, D., Yang, X., Yuan, W., Yue, X., Zaehle, S., Zeng, J., Zheng, B.: Global Carbon Budget 2023. Earth System Science Data **15**(12), 5301–5369 (2023) https://doi.org/10.5194/essd-15-5301-2023

[31] Talento, S., Willeit, M., Ganopolski, A.: New estimation of critical insolation–CO_2 relationship for triggering glacial inception. Climate of the Past **20**(6), 1349–1364 (2024) https://doi.org/10.5194/cp-20-1349-2024

[32] Laskar, J., Robutel, P., Joutel, F., Gastineau, M., Correia, A. C. M., Levrard, B.: A long-term numerical solution for the insolation quantities of the Earth. Astronomy & Astrophysics **428**(1), 261–285 (2004) https://doi.org/10.1051/0004-6361:20041335

[33] Lord, N.S., Ridgwell, A., Thorne, M.C., Lunt, D.J.: An impulse response function for the "long tail" of excess atmospheric CO_2 in an Earth system model. Global Biogeochemical Cycles **30**(1), 1–17 (2015) https://doi.org/10.1002/2014gb005074

[34] Kaufhold, C., Willeit, M., Liu, B., Ganopolski, A.: Assessing the lifetime of anthropogenic CO_2 and its sensitivity to different carbon cycle processes. EGUsphere **2024**, 1–51 (2024) https://doi.org/10.5194/egusphere-2024-2976 . (accepted)

[35] Munhoven, G., François, L.M.: Glacial-interglacial changes in continental weathering: Possible implications for atmospheric CO_2. In: Zahn, R., Pedersen, T.F., Kaminski, M.A., Labeyrie, L. (eds.) Carbon Cycling in the Glacial Ocean: Constraints on the Ocean's Role in Global Change. NATO ASI Series I: Global Environmental Change, vol. 17, pp. 39–58. Springer, Berlin (1994). https://doi.org/10.1007/978-3-642-78737-9_3

[36] Willeit, M., Ilyina, T., Liu, B., Heinze, C., Perrette, M., Heinemann, M., Dalmonech, D., Brovkin, V., Munhoven, G., Börker, J., Hartmann, J., Romero-Mujalli, G., Ganopolski, A.: The Earth system model CLIMBER-X v1.0 – Part 2: The global carbon cycle. Geoscientific Model Development **16**(12), 3501–3534 (2023) https://doi.org/10.5194/gmd-16-3501-2023

[37] Liakka, J., Lord, N.S., Kennedy-Asser, A., Lunt, D.J., Williams, C.J.R., Näslund, J.-O.: Assessing future ice-sheet variability for long-term safety of deep geological repositories. Advances in Geosciences **65**, 71–81 (2024) https://doi.org/10.5194/adgeo-65-71-2024

[38] Penman, D.E., Caves Rugenstein, J., Ibarra, D.E., Winnick, M.J.: Silicate weathering as a feedback and forcing in Earth's climate and carbon cycle. Earth-Science Reviews **209**, 1–16 (2020) https://doi.org/10.1016/j.earscirev.2020.103298

[39] Hilton, R.G.: Earth's persistent thermostat. Science **379**(6630), 329–330 (2023) https://doi.org/10.1126/science.adf3379

[40] Brovkin, V., Ganopolski, A., Archer, D., Munhoven, G.: Glacial CO_2 cycle as a succession of key physical and biogeochemical processes. Climate of the Past **8**(1), 251–264 (2012) https://doi.org/10.5194/cp-8-251-2012

[41] Willeit, M. and Ganopolski, A. and Calov, R. and Brovkin, V.: Mid-Pleistocene transition in glacial cycles explained by declining CO_2 and regolith removal. Science Advances **5**(4), 1–8 (2019) https://doi.org/10.1126/sciadv.aav7337

[42] Foster, G.L., Vance, D.: Negligible glacial–interglacial variation in continental chemical

weathering rates. Nature **444**(7121), 918–921 (2006) https://doi.org/10.1038/nature05365

[43] Hilton, R.G., West, A.J.: Mountains, erosion and the carbon cycle. Nature Reviews Earth & Environment **1**(6), 284–299 (2020) https://doi.org/10.1038/s43017-020-0058-6

[44] Zuo, H., Liu, Y., Li, G., Xu, Z., Zhao, L., Guo, Z., Hu, Y.: A revised model of global silicate weathering considering the influence of vegetation cover on erosion rate. Geoscientific Model Development **17**(9), 3949–3974 (2024) https://doi.org/10.5194/gmd-17-3949-2024

[45] Vavrus, S.J., He, F., Kutzbach, J.E., Ruddiman, W.F., Tzedakis, P.C.: Glacial inception in Marine Isotope Stage 19: An orbital analog for a natural Holocene climate. Scientific Reports **8**(1), 1–12 (2018) https://doi.org/10.1038/s41598-018-28419-5

[46] Bagge, M., Klemann, V., Steinberger, B., Latinović, M., Thomas, M.: Glacial-isostatic adjustment models using geodynamically constrained 3D Earth structures. Geochemistry, Geophysics, Geosystems **22**(11), 1–21 (2021) https://doi.org/10.1029/2021gc009853

[47] Dansgaard, W., Johnsen, S.J., Clausen, H.B., Dahl-Jensen, D., Gundestrup, N.S., Hammer, C.U., Hvidberg, C.S., Steffensen, J.P., Sveinbjörnsdottir, A.E., Jouzel, J., Bond, G.: Evidence for general instability of past climate from a 250-kyr ice-core record. Nature **364**, 218–220 (1993) https://doi.org/10.1038/364218a0

[48] Ganopolski, A., Rahmstorf, S.: Rapid changes of glacial climate simulated in a coupled climate model. Nature **409**, 153–158 (2001) https://doi.org/10.1038/35051500

[49] Willeit, M., Ganopolski, A., Edwards, N.R., Rahmstorf, S.: Surface buoyancy control of millennial-scale variations in the Atlantic meridional ocean circulation. Climate of the Past **20**(12), 2719–2739 (2024) https://doi.org/10.5194/cp-20-2719-2024

[50] Svendsen, J.I., Alexanderson, H., Astakhov, V.I., Demidov, I., Dowdeswell, J.A., Funder, S., Gataullin, V., Henriksen, M., Hjort, C., Houmark-Nielsen, M., Hubberten, H.W., Ingólfsson, Ó., Jakobsson, M., Kjær, K.H., Larsen, E., Lokrantz, H., Lunkka, J.P., Lyså, A., Mangerud, J., Matiouchkov, A., Murray, A., Möller, P., Niessen, F., Nikolskaya, O., Polyak, L., Saarnisto, M., Siegert, C., Siegert, M.J., Spielhagen, R.F., Stein, R.: Late Quaternary ice sheet history of northern Eurasia. Quaternary Science Reviews **23**(11–13), 1229–1271 (2004) https://doi.org/10.1016/j.quascirev.2003.12.008

[51] Lambeck, K., Purcell, A., Funder, S., Kjær, K.H., Larsen, E., Möller, P.: Constraints on the Late Saalian to early Middle Weichselian ice sheet of Eurasia from field data and rebound modelling. Boreas **35**(3), 539–575 (2006) https://doi.org/10.1080/03009480600781875

[52] Batchelor, C.L., Margold, M., Krapp, M., Murton, D.K., Dalton, A.S., Gibbard, P.L., Stokes, C.R., Murton, J.B., Manica, A.: The configuration of Northern Hemisphere ice sheets through the Quaternary. Nature Communications **10**(1), 3713 (2019) https://doi.org/10.1038/s41467-019-11601-2

[53] Bahadory, T., Tarasov, L., Andres, H.: Last glacial inception trajectories for the Northern Hemisphere from coupled ice and climate modelling. Climate of the Past **17**(1), 397–418 (2021) https://doi.org/10.5194/cp-17-397-2021

[54] Dalton, A.S., Stokes, C.R., Batchelor, C.L.: Evolution of the Laurentide and Innuitian ice sheets prior to the last glacial maximum (115 ka to 25 ka). Earth-Science Reviews **224** (2022) https://doi.org/10.1016/j.earscirev.2021.103875

[55] Archer, D., Kheshgi, H., Maier-Reimer, E.: Multiple timescales for neutralization of fossil fuel CO_2. Geophysical Research Letters **24**(4), 405–408 (1997) https://doi.org/10.1029/97gl00168

[56] Archer, D., Eby, M., Brovkin, V., Ridgwell, A., Cao, L., Mikolajewicz, U., Caldeira, K.,

Matsumoto, K., Munhoven, G., Montenegro, A., al.: Atmospheric lifetime of fossil fuel carbon dioxide. Annual Review of Earth and Planetary Sciences **37**(1), 117–134 (2009) https://doi.org/10.1146/annurev.earth.031208.100206

[57] Lord, N.S., Lunt, D., Thorne, M.: Modelling changes in climate over the next 1 million years. Technical report, Sweden (2019). SKB-TR-19-09. https://www.skb.com/publication/2494175/

[58] Robinson, A., Calov, R., Ganopolski, A.: Multistability and critical thresholds of the Greenland ice sheet. Nature Climate Change **2**(6), 429–432 (2012) https://doi.org/10.1038/nclimate1449

[59] Bochow, N., Poltronieri, A., Robinson, A., Montoya, M., Rypdal, M., Boers, N.: Overshooting the critical threshold for the greenland ice sheet. Nature **622**(7983), 528–536 (2023) https://doi.org/10.1038/s41586-023-06503-9

[60] Höning, D., Willeit, M., Calov, R., Klemann, V., Bagge, M., Ganopolski, A.: Multistability and transient response of the Greenland ice sheet to anthropogenic CO_2 emissions. Geophysical Research Letters **50**(6), 1–11 (2023) https://doi.org/10.1029/2022GL101827

[61] Hodell, D.A., Crowhurst, S.J., Lourens, L., Margari, V., Nicolson, J., Rolfe, J.E., Skinner, L.C., Thomas, N.C., Tzedakis, P.C., Mleneck-Vautravers, M.J., Wolff, E.W.: A 1.5-million-year record of orbital and millennial climate variability in the North Atlantic. Climate of the Past **19**(3), 607–636 (2023) https://doi.org/10.5194/cp-19-607-2023

[62] Khodri, M., Ramstein, G., Paillard, D., Duplessy, J.C., Kageyama, M., Ganopolski, A.: Modelling the climate evolution from the last interglacial to the start of the last glaciation: The role of Arctic Ocean freshwater budget. Geophysical Research Letters **30**(12), 1–4 (2003) https://doi.org/10.1029/2003GL017108

[63] Yin, Q.Z., Wu, Z.P., Berger, A., Goosse, H., Hodell, D.: Insolation triggered abrupt weakening of Atlantic circulation at the end of interglacials. Science **373**(6558), 1035–1040 (2021) https://doi.org/10.1126/science.abg1737

[64] Lofverstrom, M., Thompson, D.M., Otto-Bliesner, B.L., Brady, E.C.: The importance of Canadian Arctic Archipelago gateways for glacial expansion in Scandinavia. Nature Geoscience **15**(6), 482–488 (2022) https://doi.org/10.1038/s41561-022-00956-9

[65] Hülse, D., Ridgwell, A.: Instability in the geological regulation of Earth's climate. EarthArXiv (2024) https://doi.org/10.31223/x5f13x

[66] Lüthi, D., Le Floch, M., Bereiter, B., Blunier, T., Barnola, J.-M., Siegenthaler, U., Raynaud, D., Jouzel, J., Fischer, H., Kawamura, K., Stocker, T.F.: High-resolution carbon dioxide concentration record 650,000–800,000 years before present. Nature **453**(7193), 379–382 (2008) https://doi.org/10.1038/nature06949

[67] Willeit, M., Ganopolski, A., Robinson, A., Edwards, N.R.: The Earth system model CLIMBER-X v1.0 – Part 1: Climate model description and validation. Geoscientific Model Development **15**(14), 5905–5948 (2022) https://doi.org/10.5194/gmd-15-5905-2022

[68] Willeit, M., Calov, R., Talento, S., Greve, R., Bernales, J., Klemann, V., Bagge, A. M.and Ganopolski: Glacial inception through rapid ice area increase driven by albedo and vegetation feedbacks. Climate of the Past **20**(3), 597–623 (2024) https://doi.org/10.5194/cp-20-597-2024

[69] Edwards, N.R., Willmott, A.J., Killworth, P.D.: On the role of topography and wind stress on the stability of the thermohaline circulation. Journal of Physical Oceanography **28**(5), 756–778 (1998) https://doi.org/10.1175/1520-0485(1998)028⟨0756:OTROTA⟩2.0.CO;2

[70] Edwards, N.R., Marsh, R.: Uncertainties due to transport-parameter sensitivity in an efficient 3-D ocean-climate model. Climate Dynamics **24**(4), 415–433 (2005) https://doi.org/10.1007/s00382-004-0508-8

[71] Willeit, M., Ganopolski, A.: PALADYN v1.0, a comprehensive land surface–vegetation–carbon cycle model of intermediate complexity. Geoscientific Model Development **9**(10), 3817–3857 (2016) https://doi.org/10.5194/gmd-9-3817-2016

[72] Heinze, C., Maier-Reimer, E.: The Hamburg oceanic carbon cycle circulation model version "HAMOCC2s" for long time integrations. Technical Report 20, Deutsches Klimarechenzentrum, Modellbetreuungsgruppe, Hamburg, Germany (1999). TRN DE00G1064, ISSN 0940-9327

[73] Ilyina, T., Six, K.D., Segschneider, J., Maier-Reimer, E., Li, H., Núñez-Riboni, I.: The global ocean biogeochemistry model HAMOCC: Model architecture and performance as component of the MPI-Earth system model in different CMIP5 experimental realizations. Journal of Advances in Modeling Earth Systems **5**(2), 287–315 (2013) https://doi.org/10.1029/2012MS000178

[74] Mauritsen, T., Bader, J., Becker, T., Behrens, J., Bittner, M., Brokopf, R., Brovkin, V., Claussen, M., Crueger, T., Esch, M., Fast, I., Fiedler, S., Fläschner, D., Gayler, V., Giorgetta, M., Goll, D.S., Haak, H., Hagemann, S., Hedemann, C., Hohenegger, C., Ilyina, T., Jahns, T., Jimenéz-de-la-Cuesta, D., Jungclaus, J., Kleinen, T., Kloster, S., Kracher, D., Kinne, S., Kleberg, D., Lasslop, G., Kornblueh, L., Marotzke, J., Matei, D., Meraner, K., Mikolajewicz, U., Modali, K., Möbis, B., Müller, W.A., Nabel, J.E.M.S., Nam, C.C.W., Notz, D., Nyawira, S.-S., Paulsen, H., Peters, K., Pincus, R., Pohlmann, H., Pongratz, J., Popp, M., Raddatz, T.J., Rast, S., Redler, R., Reick, C.H., Rohrschneider, T., Schemann, V., Schmidt, H., Schnur, R., Schulzweida, U., Six, K.D., Stein, L., Stemmler, I., Stevens, B., Storch, J.-S., Tian, F., Voigt, A., Vrese, P., Wieners, K.-H., Wilkenskjeld, S., Winkler, A., Roeckner, E.: Developments in the MPI-M Earth system model version 1.2 (MPI-ESM1.2) and its response to increasing CO_2. Journal of Advances in Modeling Earth Systems **11**(4), 998–1038 (2019) https://doi.org/10.1029/2018MS001400

[75] Greve, R.: Application of a polythermal three-dimensional ice sheet model to the Greenland ice sheet: Response to steady-state and transient climate scenarios. Journal of Climate **10**(5), 901–918 (1997) https://doi.org/10.1175/1520-0442(1997)010⟨0901:AOAPTD⟩2.0.CO;2

[76] Klemann, V., Martinec, Z., Ivins, E.R.: Glacial isostasy and plate motion. Journal of Geodynamics **46**(3), 95–103 (2008) https://doi.org/10.1016/j.jog.2008.04.005

[77] Martinec, Z., Klemann, V., Wal, W., Riva, R.E.M., Spada, G., Sun, Y., Melini, D., Kachuck, S.B., Barletta, V., Simon, K., A, G., James, T.S.: A benchmark study of numerical implementations of the sea level equation in GIA modelling. Geophysical Journal International **215**(1), 389–414 (2018) https://doi.org/10.1093/gji/ggy280

[78] Kaufhold, C., Willeit, M., Talento, S., Ganopolski, A., Rockström, J.: Interplay between climate and carbon cycle feedbacks could substantially enhance future warming. Environmental Research Letters (2025) https://doi.org/10.1088/1748-9326/adb6be . (accepted)

[79] Höning, D., Willeit, M., Ganopolski, A.: Reversibility of Greenland ice sheet mass loss under artificial carbon dioxide removal scenarios. Environmental Research Letters **19**(2), 1–9 (2024) https://doi.org/10.1088/1748-9326/ad2129

[80] Meybeck, M.: Global chemical weathering of surficial rocks estimated from river dissolved loads. American Journal of Science **287**(5), 401–428 (1987) https://doi.org/10.2475/ajs.287.5.401

[81] Gaillardet, J., Dupré, B., Louvat, P., Allègre, C.J.: Global silicate weathering and CO_2

consumption rates deduced from the chemistry of large rivers. Chemical Geology **159**(1), 3–30 (1999) https://doi.org/10.1016/S0009-2541(99)00031-5

[82] Munhoven, G.: Glacial–interglacial changes of continental weathering: estimates of the related CO_2 and HCO_3^- flux variations and their uncertainties. Global and Planetary Change **33**(1), 155–176 (2002) https://doi.org/10.1016/S0921-8181(02)00068-1

[83] Amiotte Suchet, P., Probst, J.-L., Ludwig, W.: Worldwide distribution of continental rock lithology: Implications for the atmospheric/soil CO_2 uptake by continental weathering and alkalinity river transport to the oceans. Global Biogeochemical Cycles **17**(2), 1–13 (2003) https://doi.org/10.1029/2002GB001891

[84] Uchikawa, J., Zeebe, R.E.: Influence of terrestrial weathering on ocean acidification and the next glacial inception. Geophysical Research Letters **35**(23), 1–5 (2008) https://doi.org/10.1029/2008GL035963

[85] Munhoven, G., François, L.M.: Glacial-interglacial variability of atmospheric CO_2 due to changing continental silicate rock weathering: A model study. Journal of Geophysical Research: Atmospheres **101**(D16), 21423–21437 (1996) https://doi.org/10.1029/96JD01842

[86] Ludwig, W., Amiotte-Suchet, P., Probst, J.-L.: Enhanced chemical weathering of rocks during the last glacial maximum: a sink for atmospheric CO_2? Chemical Geology **159**(1), 147–161 (1999) https://doi.org/10.1016/S0009-2541(99)00038-8

[87] Wan, S., Clift, P.D., Zhao, D., Hovius, N., Munhoven, G., France-Lanord, C., Wang, Y., Xiong, Z., Huang, J., Yu, Z., Zhang, J., Ma, W., Zhang, G., Li, A., Li, T.: Enhanced silicate weathering of tropical shelf sediments exposed during glacial lowstands: A sink for atmospheric CO_2. Geochimica et Cosmochimica Acta **200**, 123–144 (2017) https://doi.org/10.1016/j.gca.2016.12.010

[88] Goudie, A.S., Viles, H.A.: Weathering and the global carbon cycle: Geomorphological perspectives. Earth-Science Reviews **113**(1), 59–71 (2012) https://doi.org/10.1016/j.earscirev.2012.03.005

[89] Spratt, R.M., Lisiecki, L.E.: A late Pleistocene sea level stack. Climate of the Past **12**(4), 1079–1092 (2016) https://doi.org/10.5194/cp-12-1079-2016

[90] Lal, R.: Carbon sequestration. Philosophical Transactions of the Royal Society B: Biological Sciences **363**(1492), 815–830 (2008) https://doi.org/10.1098/rstb.2007.2185

[91] McGlade, C., Ekins, P.: The geographical distribution of fossil fuels unused when limiting global warming to 2°C. Nature **517**(7533), 187–190 (2015) https://doi.org/10.1038/nature14016

[92] Sinet, S., Ashwin, P., Heydt, A.S., Dijkstra, H.A.: AMOC stability amid tipping ice sheets: The crucial role of rate and noise. Earth System Dynamics **15**(4), 859–873 (2024) https://doi.org/10.5194/esd-15-859-2024

[93] Ganopolski, A., Calov, R., Claussen, M.: Simulation of the last glacial cycle with a coupled climate ice-sheet model of intermediate complexity. Climate of the Past **6**(2), 229–244 (2010) https://doi.org/10.5194/cp-6-229-2010

[94] Lambeck, K., Chappell, J.: Sea level change through the last glacial cycle. Science **292**(5517), 679–686 (2001) https://doi.org/10.1126/science.1059549

[95] Stokes, C.R., Tarasov, L., Dyke, A.S.: Dynamics of the North American Ice Sheet Complex during its inception and build-up to the last glacial maximum. Quaternary Science Reviews **50**, 86–104 (2012) https://doi.org/10.1016/j.quascirev.2012.07.009

Supplementary material for: Timing of a future glaciation in view of anthropogenic climate change

Christine Kaufhold[1,2*], Matteo Willeit[1], Guy Munhoven[3], Volker Klemann[4], Andrey Ganopolski[1]

[1]Department of Earth System Analysis, Potsdam Institute for Climate Impact Research (PIK), Member of the Leibniz Association, Potsdam, 14412, Brandenburg, Germany.
[2]Institute of Physics and Astronomy, Universität Potsdam, Potsdam, 14476, Brandenburg, Germany.
[3]Dépt. d'Astrophysique, Géophysique et Océanographie, Université de Liège, Liège, 4000, Belgium.
[4]Section Earth System Modelling, Department of Geodesy, GFZ Helmholtz Centre for Geosciences, Potsdam, 14473, Brandenburg, Germany.

*Corresponding author(s). E-mail(s): kaufhold@pik-potsdam.de;
Contributing authors: willeit@pik-potsdam.de; guy.munhoven@uliege.be; volker.klemann@gfz.de; andrey.ganopolski@pik-potsdam.de;

S1 Supplementary material

Table S1 Local minima in future maximum summer insolation at 65°N and corresponding glacial inception threshold in CO_2 concentration. These correspond to the $\times$ markers indicated in Fig. 2. Local minima were calculated using the signal processing package in SciPy. The inception threshold ($CO_{2,cr}$) was calculated using the maximum summer insolation from Laskar et al. (2004) [1] and Eq. 1.

Time (kyr AP)	Maximum summer insolation at 65° N (Wm^{-2})	Inception threshold $CO_{2,cr}$ (ppm)
0	478.3	234.6
17	481.1	226.0
37	496.1	185.1
54	469.1	265.2
80	484.0	217.5
98	472.5	253.3
127	462.9	287.8
147	466.3	275.2
170	453.3	327.3
194	474.5	246.6

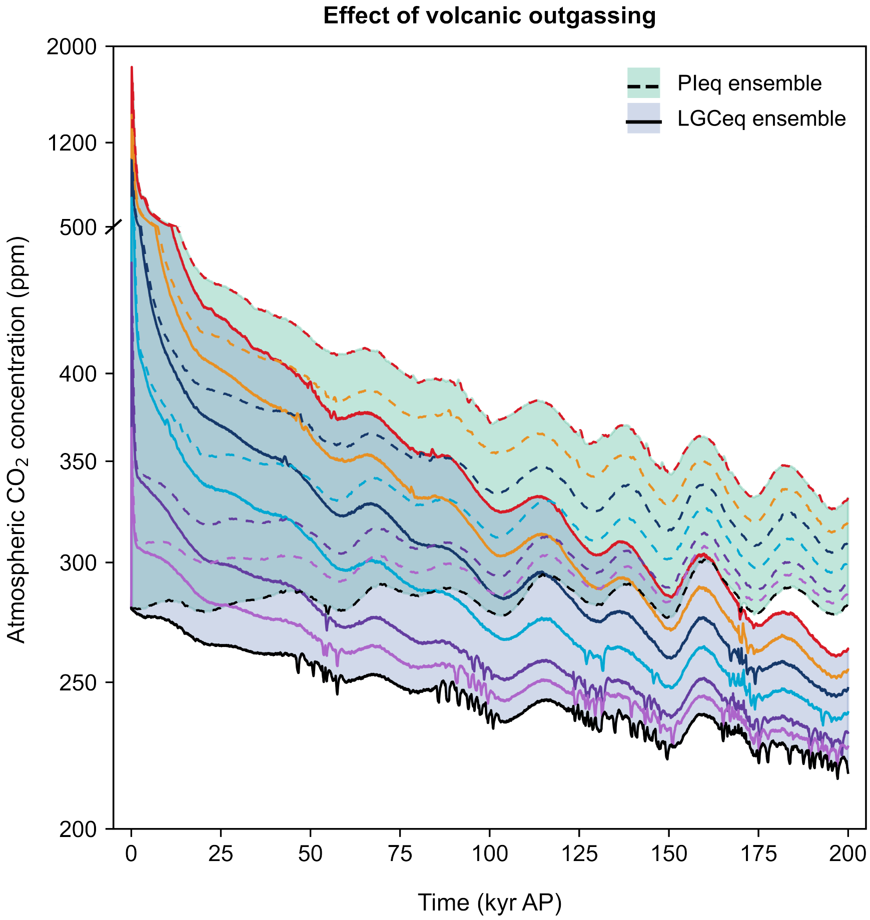

Fig. S1 Atmospheric CO_2 concentration in all experimental configurations for the ensemble of different emission scenarios. This corresponds to the experiments shown in Fig. 2d, e, and shows the effect of volcanic outgassing on atmospheric CO_2 concentration (PIeq vs. LGCeq). Colours of the trajectories correspond to the different cumulative emission scenarios shown in Fig. A2. A 300-year rolling mean was applied to the data shown here for visibility.

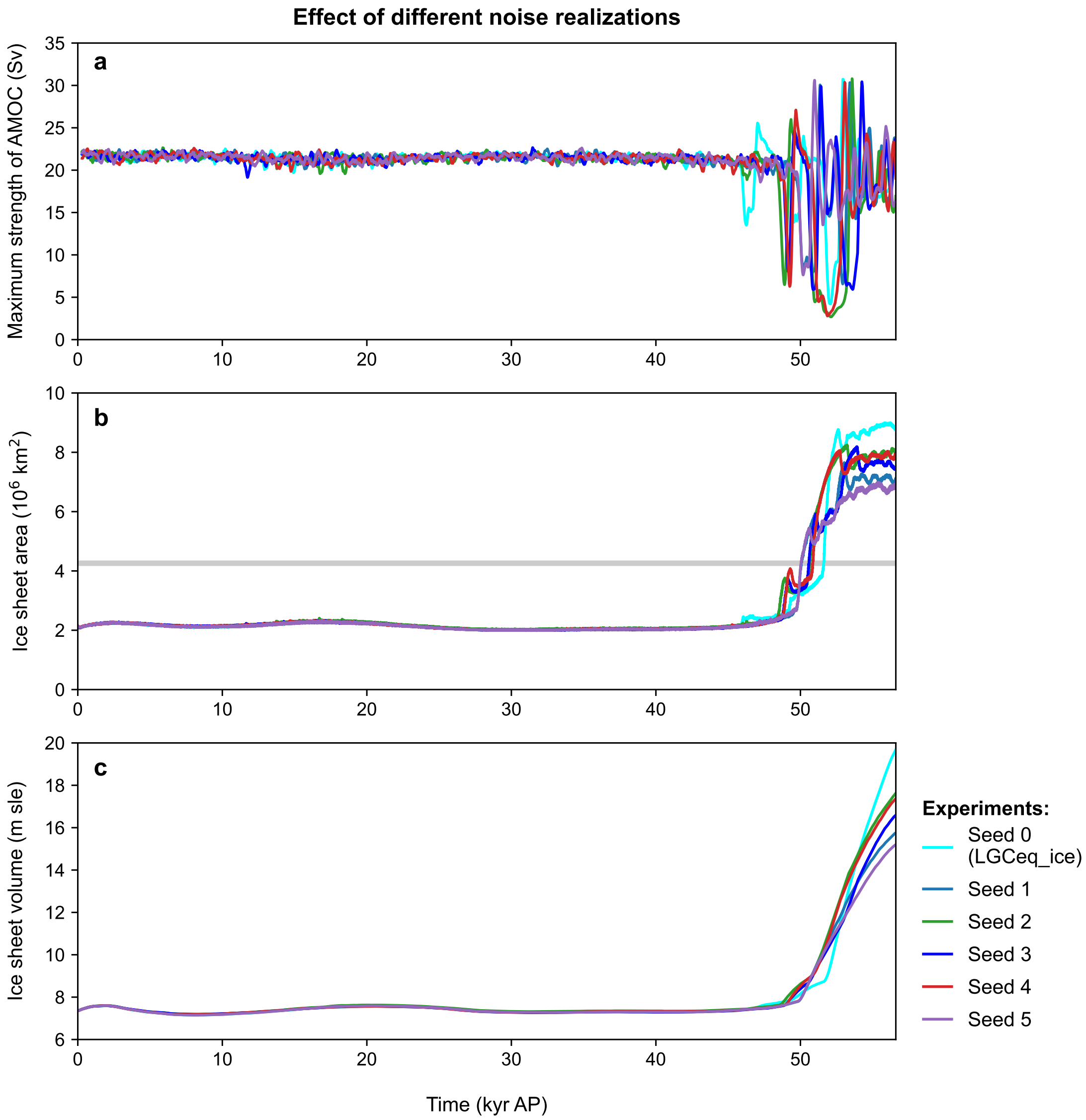

Fig. S2 Effect of different noise realizations for freshwater flux on the natural evolution of (a) AMOC, (b) ice sheet area, and (c) ice sheet volume. The experiments LGCeq_ice, LGCeq_seed1, LGCeq_seed2, LGCeq_seed3, LGCeq_seed4, and LGCeq_seed5 (Table A1) are shown here, which were performed with orbital forcing and using silicate weathering averaged over the last glacial cycle as the equilibrium condition. A 300-year rolling mean was applied to AMOC in (a) for visibility. Data is cut ∼5 kyr after the simulated timing of inception for the LGCeq_ice experiment, as discussed in Sect. 4.3 and 4.4. A doubling of present-day NH ice area ($\sim 4.26 \times 10^6$ km^2) is shown using a grey line in (b).

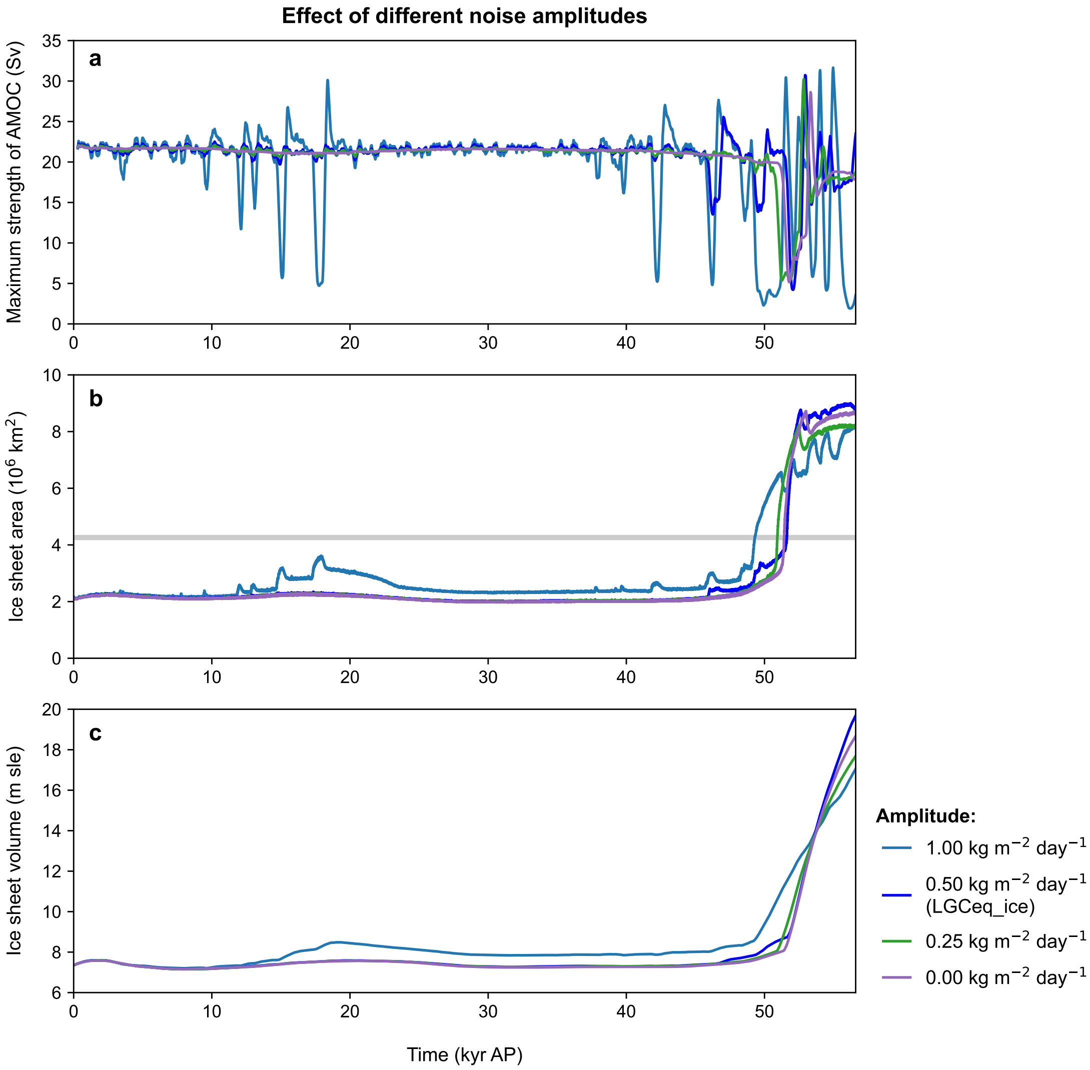

Fig. S3 Effect of different noise amplitudes for freshwater flux on the natural evolution of (a) AMOC, (b) ice sheet area, and (c) ice sheet volume. The experiments LGCeq_ice, LGCeq_n000, LGCeq_n025, and LGCeq_n100 (Table A1) are shown here, which were performed with orbital forcing and using silicate weathering averaged over the last glacial cycle as the equilibrium condition. A 300-year rolling mean was applied to AMOC in (a) for visibility. Data is cut ∼5 kyr after the simulated timing of inception for the LGCeq_ice experiment, as discussed in Sect. 4.3 and 4.4. A doubling of present-day NH ice area (∼4.26×10^6 km^2) is shown using a grey line in (b).

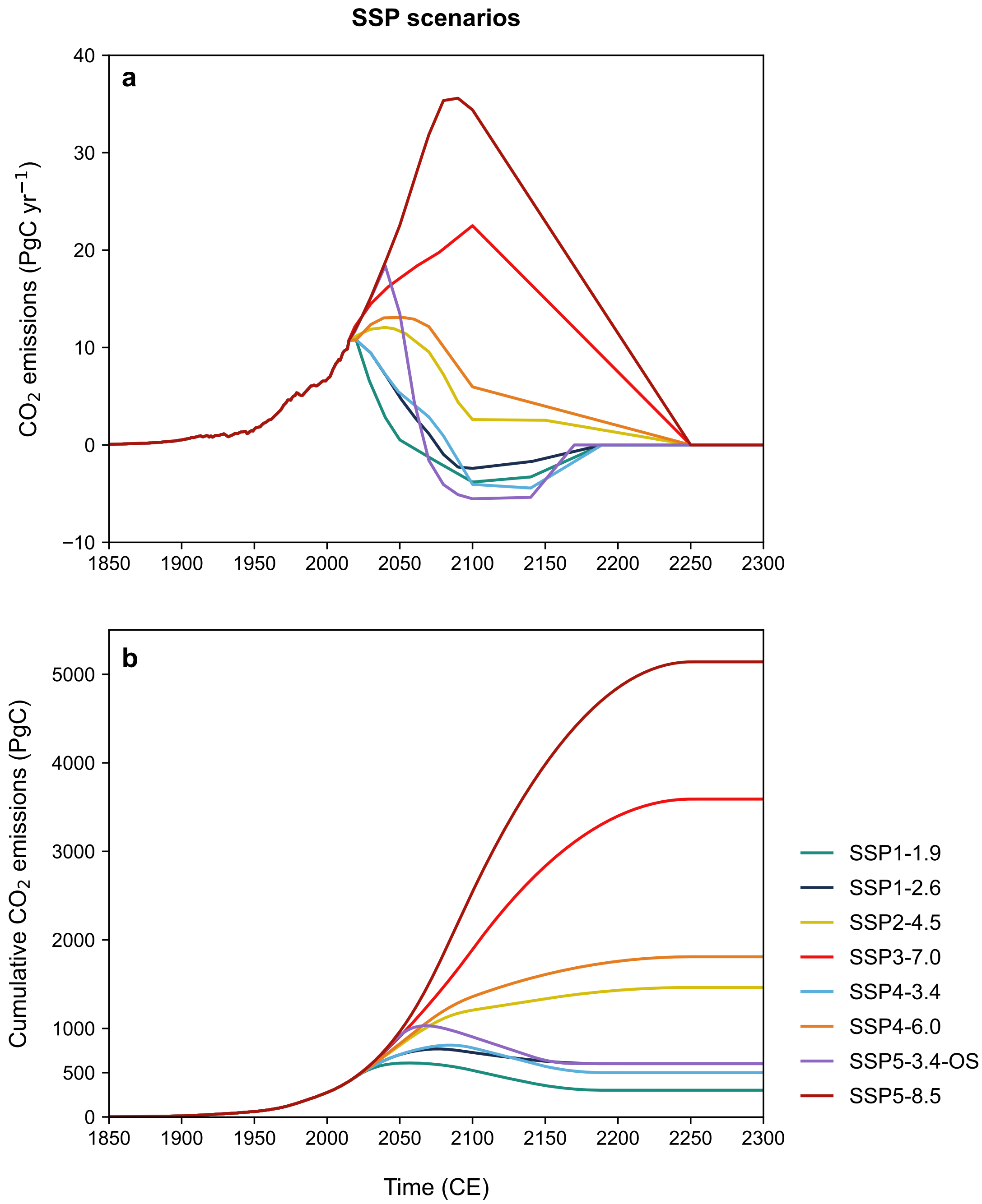

Fig. S4 The (a) CO_2 emissions and (b) cumulative CO_2 emissions for the shared socio-economic pathways (SSP). The CO_2 emission scenarios in (a) correspond to the extended pathways as shown in Meinshausen et al. (2020) [2].

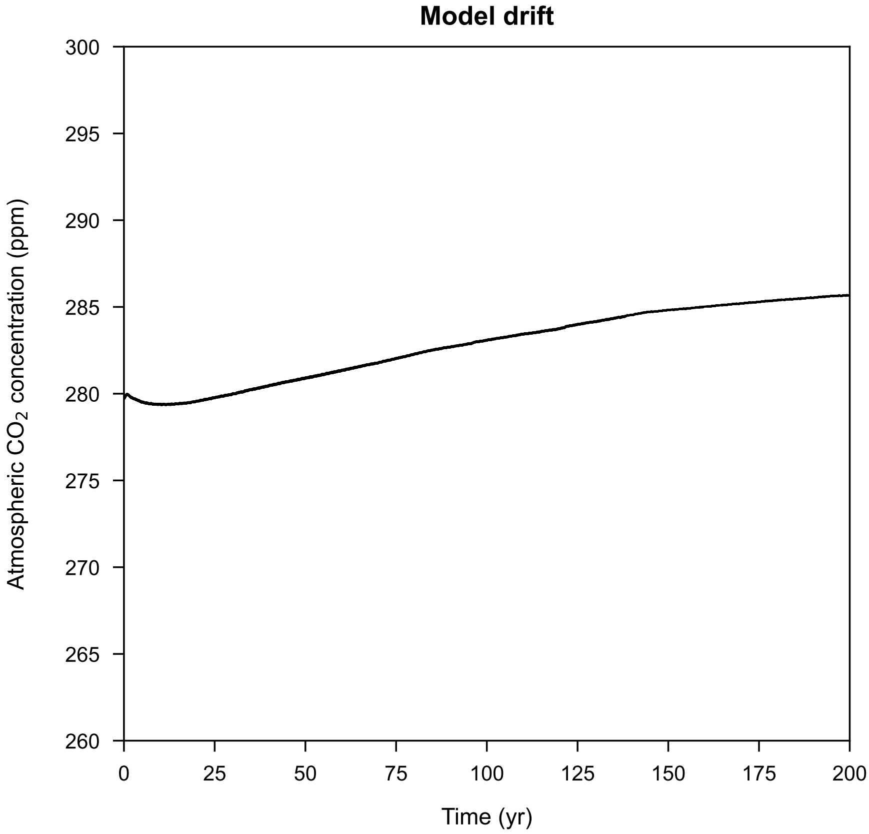

Fig. S5 Atmospheric CO_2 concentration in the PIeq_fixed experiment showing model drift in CLIMBER-X. This experiment (see Table A1) was performed without orbital forcing and noise, using the pre-industrial silicate weathering as the equilibrium condition for the next 200 kyr.

References

[1] Laskar, J., Robutel, P., Joutel, F., Gastineau, M., Correia, A. C. M., Levrard, B.: A long-term numerical solution for the insolation quantities of the Earth. Astronomy & Astrophysics **428**(1), 261–285 (2004) https://doi.org/10.1051/0004-6361:20041335

[2] Meinshausen, M., Nicholls, Z.R.J., Lewis, J., Gidden, M.J., Vogel, E., Freund, M., Beyerle, U., Gessner, C., Nauels, A., Bauer, N., Canadell, J.G., Daniel, J.S., John, A., Krummel, P.B., Luderer, G., Meinshausen, N., Montzka, S.A., Rayner, P.J., Reimann, S., Smith, S.J., Berg, M., Velders, G.J.M., Vollmer, M.K., Wang, R.H.J.: The shared socio-economic pathway (SSP) greenhouse gas concentrations and their extensions to 2500. Geoscientific Model Development **13**(8), 3571–3605 (2020) https://doi.org/10.5194/gmd-13-3571-2020